Journal of Medicinal Chemistry

Article

Discovery of a Potent, Cell Penetrant and Selective p300/CBP-Associated Factor (PCAF)/General Control Non-Derepressible 5 (GCN5) Bromodomain Chemical Probe

Philip G Humphreys, Paul Bamborough, Chun-Wa Chung, Peter D Craggs, Laurie J. Gordon, Paola Grandi, Thomas G Hayhow, Jameed Hussain, Katherine L. Jones, Matthew Lindon, Anne-Marie Michon, Jessica F Renaux, Colin J. Suckling, David F Tough, and Rab K. Prinjha

J. Med. Chem., **Just Accepted Manuscript** • DOI: 10.1021/acs.jmedchem.6b01566 • Publication Date (Web): 21 Dec 2016

Just Accepted

ACS Publications

Journal of Medicinal Chemistry is published by the American Chemical Society. 1155 Sixteenth Street N.W., Washington, DC 20036

Discovery of a Potent, Cell Penetrant and Selective p300/CBP-Associated Factor (PCAF)/General Control Non-Derepressible 5 (GCN5) Bromodomain Chemical Probe

Philip G. Humphreys,[†] Paul Bamborough,[‡] Chun-wa Chung,[‡] Peter D. Craggs,[‡] Laurie Gordon,[‡] Paola Grandi,[§] Thomas G. Hayhow,[†⊥] Jameed Hussain,[‡⊥] Katherine L. Jones,[†] Matthew Lindon,[†] Anne-Marie Michon,[§] Jessica F. Renaux,[†] Colin J. Suckling,[₸] David F. Tough,[†] Rab K. Prinjha[†]*

[†] Epigenetics Discovery Performance Unit and [‡]Platform Technology and Science, GlaxoSmithKline R&D, Stevenage, Hertfordshire SG1 2NY, United Kingdom

[§]Cellzome GmbH, Molecular Discovery Research, GlaxoSmithKline, Meyerhofstrasse 1, 69117 Heidelberg, Germany

[₸]WestCHEM, Department of Pure and Applied Chemistry, Thomas Graham Building, University of Strathclyde, 295 Cathedral Street, Glasgow, G1 1XL, United Kingdom

KEYWORDS Bromodomain, PCAF, GCN5, chemical probe, epigenetics, GSK4027, GSK4028

ABSTRACT: p300/CREB binding protein associated factor (PCAF/KAT2B) and general control non-derepressible 5 (GCN5/KAT2A) are multidomain proteins that have been implicated in retroviral infection, inflammation pathways and cancer development. However, outside of viral replication, little is known about the dependence of these effects on the C-terminal bromodomain. Herein, we report GSK4027 as a chemical probe for the PCAF/GCN5 bromodomain, together with GSK4028 as an enantiomeric negative control. The probe was optimized from a weakly potent, non-selective pyridazinone hit to deliver high potency for the PCAF/GCN5 bromodomain, high solubility, cellular target engagement and ≥18000 fold selectivity over the BET family, together with ≥70 fold selectivity over the wider bromodomain families.

INTRODUCTION

Bromodomains are structurally conserved protein modules which selectively bind to acetyl-lysine (KAc) marks on proteins and, in doing so, form part of the epigenetic regulation of gene transcription.[1] Bromodomains have recently emerged as tractable[2] and importantly, therapeutically attractive targets for a number of disease areas including inflammation and oncology.[3–6] The main body of research in the bromodomain field has focused on the BET (bromodomain and extra terminal) family and multiple small molecule inhibitors have been disclosed, as recently reviewed elsewhere.[7–10] It is of note that the publication of a variety of diverse chemical probes has enabled the wide ranging evaluation of the BET family as therapeutic targets. Historically, bromodomains outside of the BET family have received less attention in the literature, in part, due to the lack of chemical probes.[11] High quality chemical probes from diverse chemotypes have been, and will continue to be a critical component in

enabling our biological understanding of the function and target validation of the 53 non-BET members of the bromodomain phylogenetic tree.[12,13] To this end, a number of chemical probes and inhibitors for several non-BET bromodomains, for example CREBBP/EP300,[14–19] BRD7/9,[20–22] BRD9,[23] BRPF1,[24] ATAD2[25] and SMARCA2/4[26] have been disclosed, as has been recently reviewed elsewhere.[27–30] Importantly, many of these probes are readily available[31] and are already being used to elucidate the biological function of these protein reader domains in health and disease.[32–34]

KAT2B (lysine acetyl transferase 2B), also known as PCAF (p300/CBP-associated factor), is a multidomain protein containing an acetyltransferase domain, E3 ligase ubiquitination domain and a C-terminal bromodomain.[35,36] PCAF functions as a transcriptional co-activator and has been implicated in many cellular processes, including several inflammation-related pathways,[37,38] oncology,[39–41] neuro-degeneration[42] and viral replication.[43,44] KAT2A, also known as GCN5 (general control non-derepressible 5), possesses a similar domain structure and exhibits high homology with PCAF, particularly in the C-terminal bromodomain. GCN5 is reported to play important roles in cell proliferation and differentiation, nucleosome assembly as well as DNA damage repair,[45–49] and has been implicated in certain cancers, including non-small cell lung cancer and breast cancer.[47,50–52] Acetyltransferase activity is recognized to play a key role in PCAF/GCN5 function, linked to acetylation of lysine residues on both histone proteins and transcription factors.[46,53] In contrast, the function of the PCAF/GCN5 bromodomain is less well understood. Thus, while studies in yeast (which possess only a single PCAF/GCN5 family member called GCN5[54,55]) have shown that point-mutations disrupting the ability of the GCN5 bromodomain to interact with acetyl-lysine can lead to decreases in GCN5-dependent transcription and histone acetylation,[46,56] very little is known about the role of PCAF and GCN5 bromodomains in mammalian cell function.

To this end, there have been several reports concerning the development of PCAF bromodomain inhibitors. In 2005, Zhou and co-workers used an NMR screen to identify the first small molecule PCAF bromodomain inhibitor, diamine **1** (Figure 1).[57] This compound was shown to disrupt a specific interaction between PCAF and the K50Ac HIV TAT protein, which is essential for viral replication. Subsequent work to optimize this series succeeded in improving the biochemical potency, resulting in compound **2**.[58] A fragment screen against the PCAF bromodomain using surface plasmon resonance delivered fragment binders, such as amide **3** which shows 250 μM affinity for PCAF.[59] Knapp and co-workers also adopted a fragment based approach to identify PCAF binders, such as compound **4**, as potential starting points for more potent and selective PCAF inhibitors.[60]

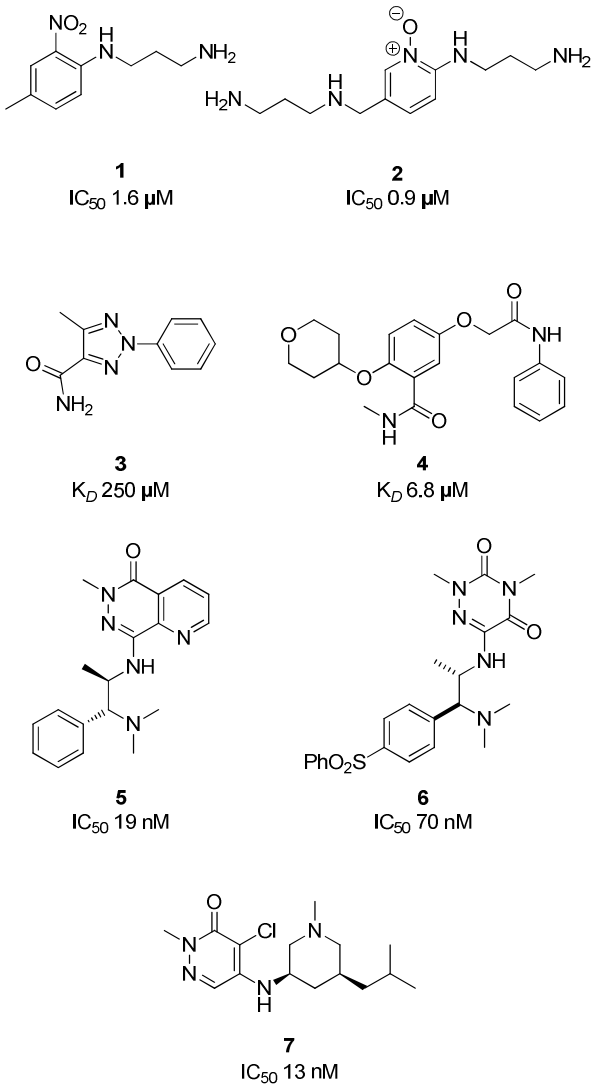

Figure 1. PCAF inhibitors showing their reported affinity to the PCAF bromodomain

Demonstrating significant improvements in potency from what had been previously reported, Genentech and Constellation Pharmaceuticals recently disclosed, in three patent applications, a number of highly potent dual PCAF/GCN5 inhibitors from three different chemotypes, as exemplified by the most active analogues from each series, compounds **5-7** (Figure 1).[61–63] During the preparation of this manuscript, the Genentech/Constellation pyridazinone patent application was published and the similarity of the pyridazinone structures, such as **7**,[63] to the

work presented in this manuscript is acknowledged. However, to the best of our knowledge, the discovery and optimization of the pyridazinone template as PCAF/GCN5 inhibitors by Genentech and Constellation scientists has not yet been reported in the peer-reviewed literature.

As detailed above, high quality chemical probes for the PCAF/GCN5 bromodomains would facilitate further elucidation of the bromodomain function. To this end, in 2011 GSK set out to generate potent and selective inhibitors of the PCAF bromodomain. Due to the profound phenotype associated with BET inhibition, it was considered that the probe should show PCAF pIC_{50} >7 with a minimum of 100-fold selectivity (2 log units) over the BET family. Cellular target engagement was critical, together with >30-fold selectivity across other bromodomain families and an understanding of broader non-bromodomain activity.[64] Another consideration was the development of a negative control, a compound with highly similar properties to the chemical probe, but with reduced activity against PCAF to provide further confidence that any phenotype could be associated with inhibition of bromodomain function.[13] Selectivity against GCN5 for the chemical probe was not expected, or indeed targeted, due to the high homology with the PCAF bromodomain mentioned previously (Figure 2c).

Here, we report the optimization of a weakly active, non-selective pyridazinone hit to deliver a potent, selective, soluble and cell penetrant chemical probe for the PCAF/GCN5 bromodomains and the enantiomeric negative control.

RESULTS AND DISCUSSION

PCAF, like the BET family, is classified as a typical bromodomain with conserved asparagine and tyrosine residues responsible for KAc recognition (Figure 2).[60,65] Comparison of the X-ray crystal structures of apo PCAF (Figure 2a) and BRD4 BD1 (Figure 2b) reveals a profound

difference in the ZA channel regions due to differences in the amino acids.[66] PCAF, like the BET family, contains a lipophilic WPF shelf (Figure 2c). However, in the PCAF bromodomain the bulky Tyr809 gatekeeper residue blocks access and creates a far narrower binding pocket when compared with BRD4 BD1. In contrast, BRD4 BD1 contains a smaller Ile146 which permits access to the WPF shelf, with binding to this lipophilic region typically observed with BET bromodomain inhibitors such as I-BET151 (Figure 2b). Another important difference is an acidic residue in the ZA loop region, Glu756 in PCAF, whose 3D equivalent in the BET family is a lipophilic leucine (BRD4 BD1 Leu92), which provides the potential for a selective interaction (*vide infra*).

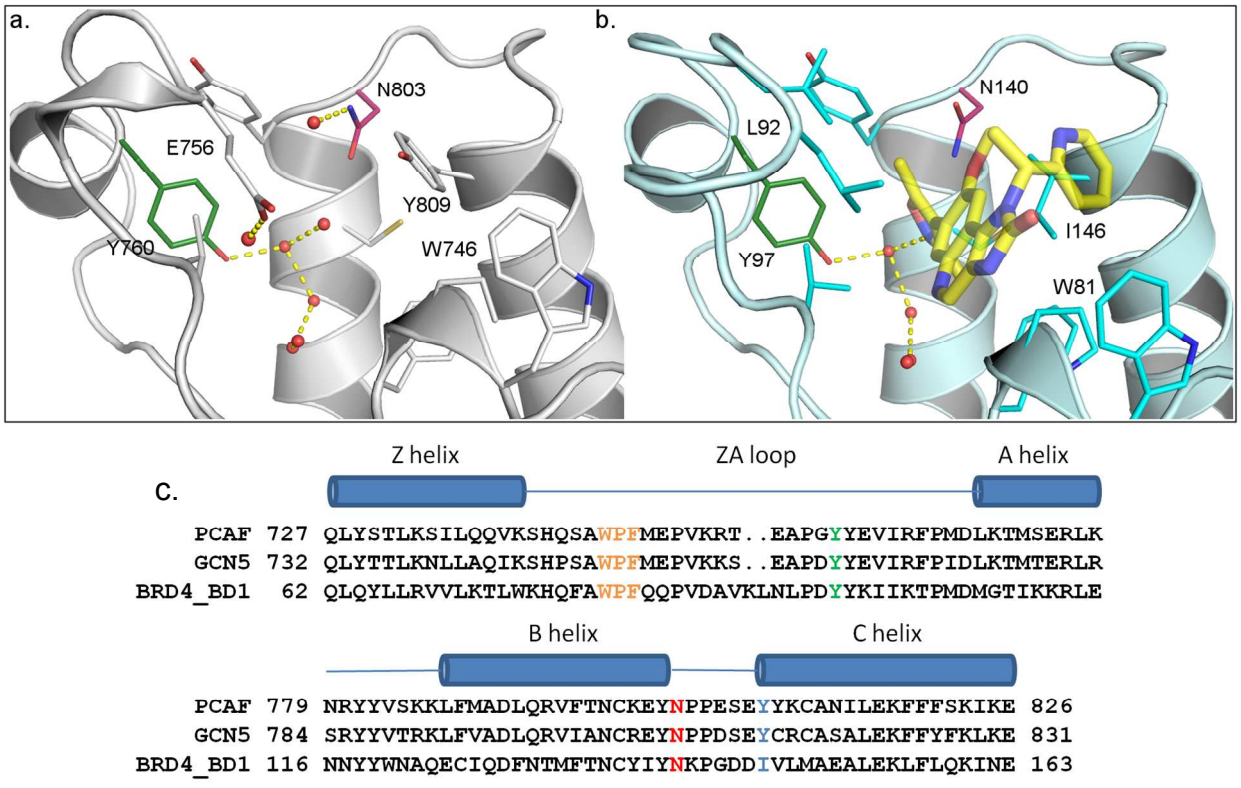

Figure 2. (a) X-ray crystal structure of apo PCAF bromodomain (pdb: 3gg3) (grey). Hydrogen-bonds are shown as yellow dashed lines and selected water molecules as red spheres; (b) X-ray crystal structure of BRD4 BD1 bromodomain (cyan) in complex with I-BET151 (pdb: 3zyu)

(yellow); (c) Sequence alignment of PCAF, GCN5 and BRD4 BD1. The WPF moiety is colored orange, the conserved acetyl-lysine-binding asparagines and tyrosine are colored red and green respectively and the gatekeeper residue is colored blue.

Discovery of the Pyridazinone Series. As previously disclosed,[67] as part of our bromodomain discovery strategy we assembled a focused set of compounds containing known and potential KAc mimetics. This set of ~30,000 compounds was screened in single shot format at 10 μM against PCAF using a fluorescence polarization assay based on a labeled small molecule promiscuous bromodomain binder. A number of single shot hits, including pyridazinone **8** were progressed to full curve analysis and an orthogonal ^{15}N-^{1}H HSQC NMR screen to rule out potential assay interference. Full curve screening of **8** in a time-resolved fluorescence resonance energy transfer (TR-FRET) assay demonstrated moderate potency with pIC_{50} 4.8 (IC_{50} 16 μM) and an encouraging ligand efficiency of 0.37 (Figure 3). Profiling compound **8** more broadly revealed equipotent activity against the BET family, with BRD4 BD1 (*N*-terminal, bromodomain 1) used as a representative member of the BET family for optimization throughout. Pyridazinone **8** also demonstrated high levels of aqueous solubility as determined by chemiluminescent nitrogen detection (CLND) and a Chrom$LogD_{pH7.4}$ 3.3. In the NMR experiment, a subset of peaks were shifted upon binding to pyridazinone **8**, consistent with interactions at the KAc binding site. Although we thought it likely that the carbonyl group would mimic the KAc hydrogen-bonding interactions to Asn803 and *via* water to Tyr809, it was unclear whether the chloro or methyl group of **8** was occupying the PCAF methyl pocket.[68]

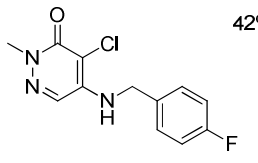

8

42% PCAF inhibition at 10 μM
PCAF pIC_{50}: 4.8
BRD4 BD1 pIC_{50}: 4.8
PCAF LE: 0.37
CLND: >502 μM
Chrom$LogD_{pH7.4}$: 3.3

Figure 3. Profile of pyridazinone hit **8**

With confirmation of PCAF binding by orthogonal assay formats, we selected pyridazinone **8** as a synthetically tractable, soluble, small and ligand efficient start point for further optimization. Initial SAR was rapidly developed around this template through either external purchase (compounds **10-12**) or straightforward S_NAr chemistry with commercially available 4,5-dichloropyridazinone **9** (Scheme 1).[69] Although the methodology typically gave a ~3:1 mixture of 4- and 5-positional isomers, substitution at the desired 5-position is favored and these products were easily separable by column chromatography.

Scheme 1[a]

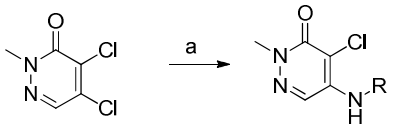

[a]Reagents and conditions: (a) RNH_2, DIPEA, DMSO, 120-130 °C, 1-5 h

SAR for the initial pyridazinone compounds are shown in Table 1. The PCAF and BRD4 BD1 binding data was generated using TR-FRET assays based on labeled small molecule bromodomain binders. Selectivity between PCAF and BRD4 BD1 is represented by a Δ, the difference between PCAF pIC_{50} and BRD4 BD1 pIC_{50}

Table 1. PCAF and BRD4 BD1 SAR for the pyridazinone series[a]

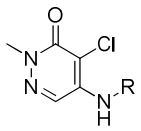

Compound	R	PCAF pIC_{50}	PCAF LE	BRD4 BD1 pIC_{50}	Δ	Chrom $Log D_{pH7.4}$

8	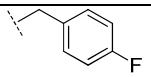	4.8	0.37	4.8	0	3.3
10	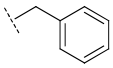	4.9	0.40	4.7	0.2	3.2
11	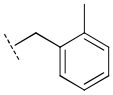	5.2	0.40	4.6	0.6	3.8
12	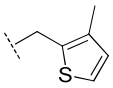	5.2	0.42	4.7	0.5	3.4
13	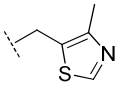	5.1	0.41	<4.3	>0.8	1.2
14	Ph	5.0	0.43	4.5	0.5	3.1
15	Me	4.7	0.59	3.9	0.8	0.4
16	*i*-Pr	4.5	0.47	<4.3	>0.2	2.2

[a]LE = (1.37 × pIC_{50}) / heavy atom count. Δ = PCAF pIC_{50} – BRD4 BD1 pIC_{50}. For statistics, see Table S1, Supporting information.

Removal of the fluoro group from **8** to give compound **10** demonstrated that the halogen had little effect on potency at either PCAF or BRD4 BD1. Substitution of the phenyl ring with a variety of groups revealed that the 2-position, in particular, afforded an increase in PCAF potency and selectivity over BRD4 BD1, for example with a 2-methyl group (compound **11**). The phenyl ring could be replaced with the bioisosteric thiophene to give **12**, which maintained PCAF potency. Introduction of the more polar thiazole ring to give **13** reduced BRD4 BD1 potency while maintaining activity at PCAF. This gave us encouragement to believe that selectivity over the BET family would potentially be achievable with the pyridazinone series.

Removal of the methylene from **10** to give phenyl **14** maintained PCAF potency with a concomitant increase of ligand efficiency. Further truncation to methyl substituted fragment **15** retained the potency of compound **8** at PCAF, together with a substantial boost in ligand efficiency (0.37 to 0.59). The added benefit of this change was the encouraging improvement in

selectivity over BRD4 BD1. Growing to *i*-Pr **16** was tolerated at the expense of ligand efficiency, with activity against BRD4 BD1 not measurable at the concentrations tested.

Initial attempts to obtain crystal structures of pyridazinones such as thiophene **12** in complex with PCAF by soaking preformed apo crystals of human PCAF bromodomain were unsuccessful. Analysis of the crystal packing around the acetyl-lysine binding site of the bromodomain suggested it may be due to the proximity of adjacent protein molecules within the crystal lattice. However, structures of PCAF from soaked crystals in complex with smaller compounds such as fragment **15** were successful, presumably as the absence of larger groups prevented disruption of protein contacts required to maintain the crystal integrity. A structure was also obtained of fragment **15** in complex with BRD4 BD1 for comparison (Figure 4).

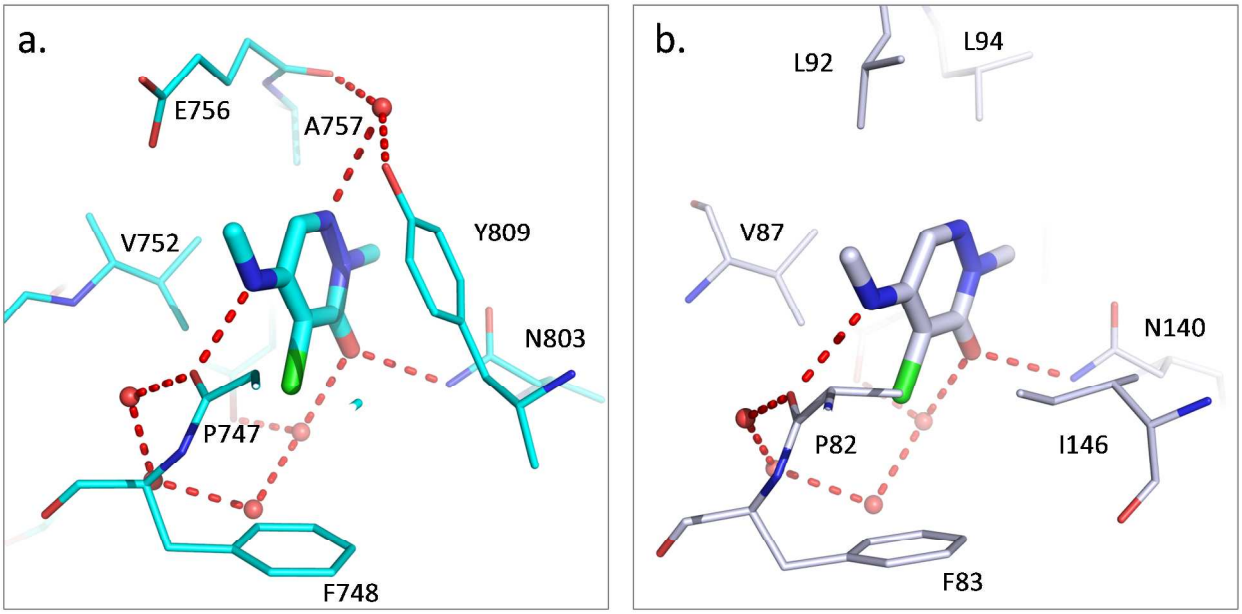

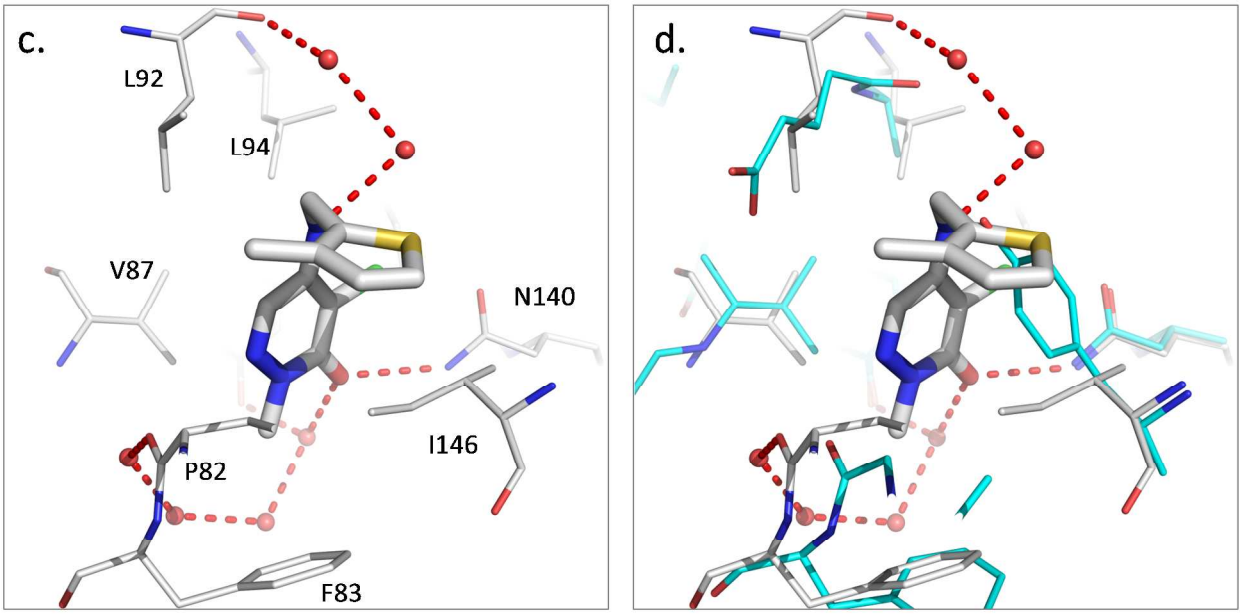

Figure 4. X-ray crystal structures of (a) PCAF bromodomain (cyan) in complex with **15** (cyan); (b) BRD4 BD1 bromodomain (grey) in complex with **15** (grey); (c) BRD4 BD1 bromodomain (grey) in complex with **12** (grey); (d) overlay of BRD4 BD1 bromodomain (grey) in complex with **12** (grey) and PCAF bromodomain (cyan). Hydrogen-bonds are shown as red dashed lines and selected water molecules as red spheres.

The overall structure of **15** bound to PCAF showed a similar protein conformation to the published apo structure,[66] with a slight rotation of the gatekeeper Tyr809 that allows a face-to-face aromatic interaction with the pyridazinone core. The ZA loop does show slight movements between bound and unbound structures: the sidechains are observed in the same conformation, except Val752 which is rotated ~120°, although this rotated conformation has been seen in other structures with fragments bound.[60] A number of hydrogen-bonds are observed between fragment **15** and the PCAF bromodomain including the expected hydrogen-bond *via* the carbonyl group to the side-chain NH_2 group of Asn803 (Figure 4a). Additionally, a shorter hydrogen-bond was also made to a conserved water molecule bound by Tyr760. A further hydrogen-bond between the NH group of **15** and the backbone carbonyl group of Pro747 was also observed. Finally, the

pyridazinone ring N made a long through-water hydrogen-bond to gatekeeper Tyr809 and the backbone carbonyl of Glu756. Interestingly, the chloro group acted as the methyl mimetic, sitting in the small pocket surround by four crystallographically conserved waters. The pyridazinone NMe group sits adjacent to Tyr802 with excellent shape complementarity to the binding pocket.

In comparison, the structure of **15** in complex with BRD4 BD1 shows the same hydrogen-bonding interactions as observed in PCAF (Figure 4b). The canonical hydrogen-bond between the carbonyl group to Asn140 is observed, together with a through-water hydrogen-bond to Tyr97. A hydrogen-bond to the backbone carbonyl group of Pro82 by the pendant NH group is also seen, together with the chloro group sitting in the methyl pocket. Presumably the difference in potency of fragment **15** between the two proteins is related to the positive aromatic interactions with Tyr809 in PCAF that are not possible in BRD4 BD1 due to the Ile146 gatekeeper residue.

To further understand the binding mode of these compounds, thiophene **12** was selected for crystallography with BRD4 BD1. As discussed above, crystallography in PCAF was unsuccessful with this compound. Intriguingly, a flipped binding mode in BRD4 BD1 was observed with thiophene **12** when compared to fragment **15** (compare Figure 4b and 4c). Although the carbonyl group made the expected interactions with Asn140 and Tyr97 *via* a water molecule, the chloro group was no longer sitting in the methyl pocket. The pyridazine core had flipped 180^{o} and the pendant methyl group was now sitting in the methyl pocket. As a result, the NH group no longer made a hydrogen-bonding interaction with Pro82 and appeared to be bound to bulk solvent. The thiophene ring was now sitting on the lipophilic WPF shelf, presumably driving the change in binding mode. This binding mode observed in BRD4 BD1 would not be

possible in PCAF due to the difference in gatekeeper residue; the bulky Tyr809 in PCAF would block the thiophene ring from occupying the same vector (Figure 4d). This structure also explained the increase in selectivity over BRD4 BD1 when moving from a thiophene ring to a thiazole ring (compare compound **12** and compound **13**, Table 1). Presumably, the more polar thiazole (ChromLog$D_{pH7.4}$ 1.2) is less well tolerated on the lipophilic WPF shelf than the thiophene (ChromLog$D_{pH7.4}$ 3.4), which drives a reduction in BET activity.

Optimization of the aniline group. With an understanding of how to drive selectivity over the BET family with the use of polar aryls rings, a number of 'benzyl' analogues were accessed to try to improve PCAF activity. Unfortunately, no increases in PCAF potency were observed, despite repeated efforts, which led us to move away from the 'benzyl' substituted pyridazinone sub-series. Optimization was far more successfully conducted using aniline **14** as the lead. Although lacking a crystal structure of **14** bound to PCAF, we hypothesized that the phenyl ring may provide suitable vectors to interact with Glu756 *via* a basic functionality. As discussed above, the analogous residue in 3D space in BRD4 BD1 (and the rest of the BET bromodomain family) is a leucine.

Although the S_NAr synthetic route described above was suitable for chemistry with simple anilines (Scheme 1), this approach was less successful with more elaborated nucleophiles. As such, an alternative route was developed using a chemoselective Buchwald-Hartwig coupling with known 4-chloro-5-iodo pyridazinone **17** to facilitate access to the desired targets (Scheme 2).[70]

Scheme 2[a]

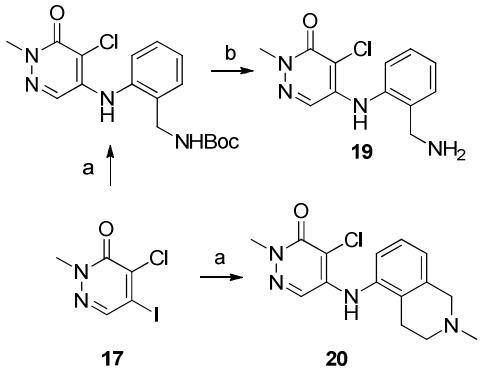

[a]Reagents and conditions: (a) RNH_2, (±)-BINAP, $Pd(OAc)_2$, Cs_2CO_3, PhMe, 80 °C; (b) HCl, IPA, rt, 2 h, 73%.

Table 2. SAR for aniline substituted pyridazinones[a]

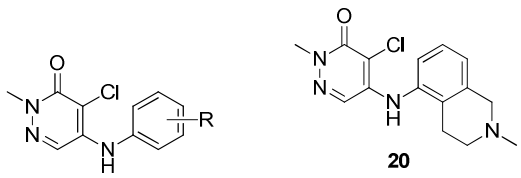

Compound	R	PCAF pIC_{50}	PCAF LE	BRD4 BD1 pIC_{50}	BRD9 pIC_{50}	Δ	Chrom Log$D_{pH7.4}$
14	H	5.0	0.43	4.5	5.6	0.5	3.1
18	3-Me	5.2	0.42	4.8	5.9	0.4	3.8
19	2-CH_2NH_2	6.0	0.46	<4.3	n.d.	>1.7	0.3
20	see above	6.5	0.42	<4.3	5.7	>2.2	1.7

[a]LE = (1.37 × pIC_{50}) / heavy atom count. Δ = PCAF pIC_{50} – BRD4 BD1 pIC_{50}. n.d.=not determined. For statistics, see Table S1, Supporting information.

Although substitution of the phenyl ring with an alkyl group had little effect on either PCAF potency or selectivity over BRD4 BD1 (Compound **18**, Table 2), we were hugely encouraged with compound **19** containing a pendant amine group. A substantial jump in PCAF potency was observed, together with an increase in ligand efficiency upon addition of this basic moiety (compare **14** and **19**). Confirming our design hypothesis that a basic group may drive selectivity over the BET family, a dramatic jump in the Δ value to >50 fold selectivity was seen. Due to the low Chrom Log$D_{pH7.4}$ of amine **19**, more lipophilic analogues were investigated to ensure cell

permeability. The potency and selectivity was driven further with THIQ (tetra-hydroisoquinoline) **20** which displayed ~300 nM potency toward PCAF with over 100 fold selectivity over BRD4 BD1. With a ChromLog$D_{pH7.4}$ 1.7, ≥660 μM CLND aqueous solubility and 377 nm/s artificial membrane permeability (AMP), we felt that THIQ **20** may be suitable, or very close to being suitable as a chemical probe for the PCAF bromodomain. However, as we profiled this compound more broadly, substantial activity against BRD9 (pIC_{50} 5.7, IC_{50} 2 μM) was uncovered. Although a crystal structure of an elaborated pyridazinone in complex with PCAF still eluded us at this stage, the more robust BRD9 crystallographic system was used to understand the interactions driving potency against this undesired bromodomain off-target (Figure 5).

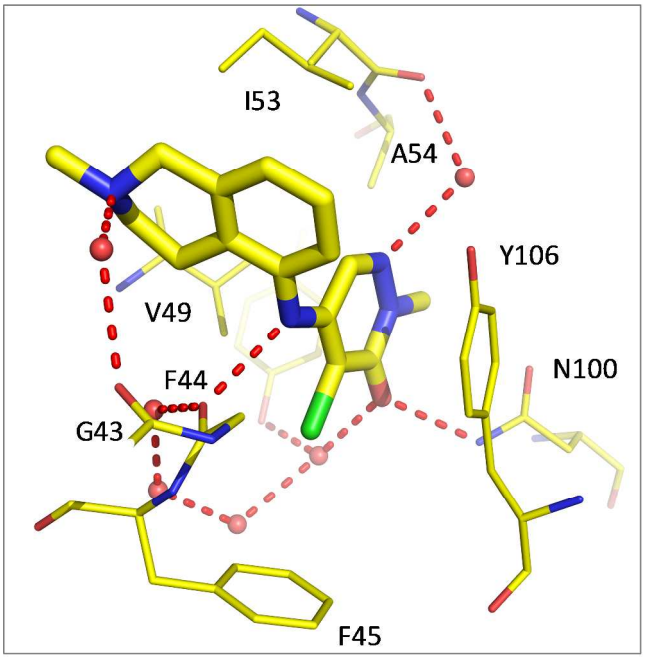

Figure 5. X-ray crystal structures of BRD9 bromodomain (yellow) in complex with **20** (yellow). Hydrogen-bonds are shown as red dashed lines and selected water molecules as red spheres.

BRD9, in contrast to the BET family, but in a similar manner to PCAF contains a Tyr gatekeeper residue. The shape created by this residue drives a similar deep, narrow binding

pocket to PCAF and, as such, the pyridazone core of THIQ **20** makes face-to-face aromatic interactions with Tyr106 in BRD9. The canonical hydrogen-bonding interactions of KAc and its mimetics are made by the pyridazinone carbonyl directly to Asn100 and *via* water to Tyr57. As in the structures of fragment **15** in complex with PCAF and BRD4 BD1 (see Figure 4), the NH group makes a hydrogen-bonding interaction with a backbone carbonyl, in this case, Phe44. The basic amine makes a through-water hydrogen-bond to the Gly43 backbone carbonyl. Additionally, the pyridazinone ring N interacts with Ile53 *via* a long through-water hydrogen-bond. As discussed above, the THIQ was designed to target a specific interaction with PCAF Glu756 for potency and selectivity over the BET family, with the data suggesting that this was possible (Table 2). In BRD9, the comparable residue in 3D space is the neutral and hydrophobic Ile53 and as expected, no specific interaction is made.

Optimization of the basic group. Attempts to overcome activity at BRD9 and engender selectivity *via* optimization of the aniline or THIQ groups were unfortunately unsuccessful. As such, we turned our attention back to the initial SAR compounds (Table 1). Screening several of these compounds against BRD9 revealed an interesting trend (Table 3).

Table 3. SAR at BRD9 for select pyridazinones[a]

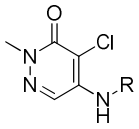

Compound	R	PCAF pIC_{50}	BRD9 pIC_{50}	Δ
13	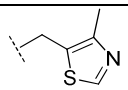	5.1	5.9	–0.8
14	Ph	5.0	5.6	–0.6
16	*i*-Pr	4.5	<4.3	>0.2

[a] Δ = PCAF pIC_{50} – BRD9 pIC_{50}. For statistics, see Table S1, Supporting information.

Thiazole **13**, despite promising selectivity against BRD4 BD1 (see Table 1), was actually substantially more potent against BRD9. Aniline **14** also showed increased potency against BRD9 when compared to PCAF, however, *i*-Pr substituted compound **16** showed a bias over BRD9. In comparison to the WPF motif (Trp746, Pro747, Phe748) in PCAF, BRD9 contains a HGFF motif (His42, Gly43, Phe44, Phe45). We hypothesize that the bulky branched sp^3 moiety linked to the NH group is not tolerated in BRD9 due to Phe44, which sits almost perpendicular to Trp746 in PCAF and creates a more restricted binding site. In comparison, thiazole **13** which contains a more flexible methylene substituent and aniline **14**, with a planer aryl ring are better accommodated within the narrow BRD9 binding site.

Encouraged by the hint of selectivity over BRD9 observed with **16**, we choose this motif to continue our optimization and accessed a selection of cyclic amines targeting the PCAF Glu756 residue (Table 4). As before, straightforward S_NAr chemistry with the appropriate amines was suitable to access the desired pyridazinone targets (Scheme 1).

Table 4. Amine substituted pyridazinones[a]

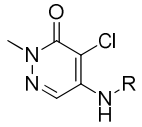

Compound	R	PCAF pIC_{50}	PCAF LE	BRD4 BD1 pIC_{50}	BRD9 pIC50	Δ	Chrom Log$D_{pH7.4}$
16	*i*-Pr	4.5	0.47	<4.3	<4.3	>0.2	2.2
21	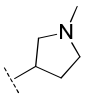	4.8	0.41	<4.3	n.d.	>0.5	–0.1
22	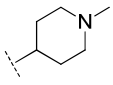	4.8	0.39	<4.3	<4.3	>0.5	–0.3
23	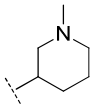	5.9	0.48	<4.3	<4.3	>1.6	0.6

(*R*)-23	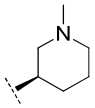	6.3	0.51	<4.3[b]	<4.3	>2	0.6
(*S*)-23	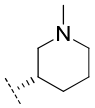	5.2	0.42	<4.3	<4.3	>0.9	0.6

[a]LE (1.37 × pIC_{50}) / heavy atom count. Δ = PCAF pIC_{50} – BRD4 BD1 pIC_{50}. n.d.=not determined. For statistics, see Table S1, Supporting information. [b]Data is 7/8 test occasions, pIC_{50} 4.8 on 1/8 test occasions.

The position of the basic amine was critical to PCAF activity with pyrrolidine **21** and 4-substituted piperidine **22** both showing little difference in profile when compared to *i*-Pr **16** (Table 3). In contrast, 3-substituted racemic piperidine **23** demonstrated a substantial increase in PCAF potency while maintaining the high ligand efficiency seen with *i*-Pr fragment **16**. Critically, the increase in PCAF potency also improved selectivity over both BRD4 BD1 and BRD9. Independent synthesis of the two enantiomers with the requisite chiral amines (see Supporting Information for details) demonstrated that the majority of the PCAF activity resided within **(*R*)-23**, with **(*S*)-23** showing 10 fold less potency. Critically, **(*R*)-23** also maintained selectivity over BRD9 and BRD4 BD1, with activity against these undesired targets below the levels of quantification at the concentrations tested.

In our attempts to establish a more robust crystallographic system for PCAF, we also explored the mouse orthologue, which differs to human in seven amino acids outside of the preserved KAc binding. For some compounds the mouse PCAF bromodomain was more successful in delivering co-crystal structures. For example the crystal structure of an elaborated pyridazinone, **(*R*)-23**, bound to mouse PCAF was obtained (Figure 6a).

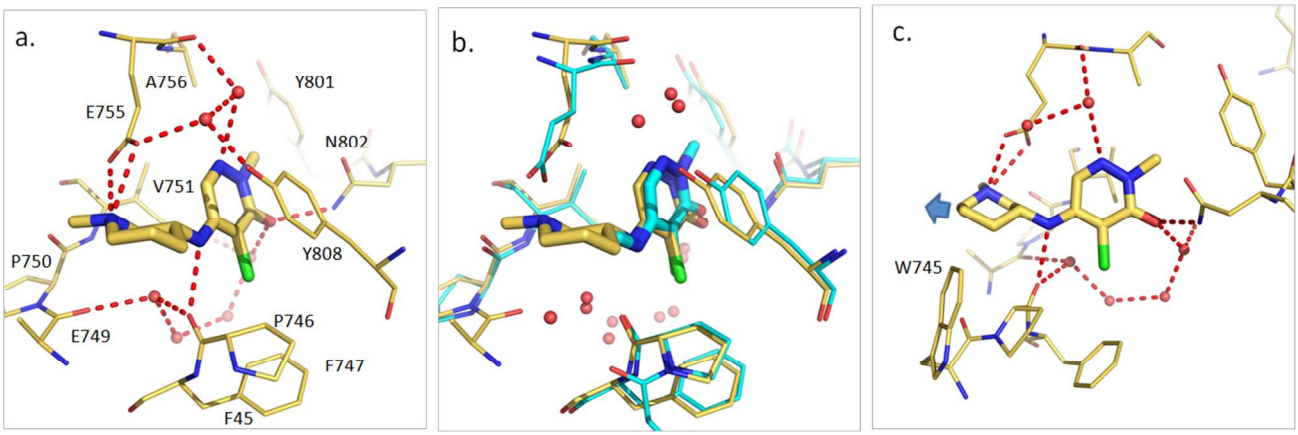

Figure 6. X-ray crystal structures of (a) mouse PCAF bromodomain (yellow) in complex with **(*R*)-23** (yellow) (b) Overlay between mouse PCAF bromodomain (yellow) in complex with **(*R*)-23** (yellow) and human PCAF bromodomain (cyan) in complex with **15** (cyan). (c) PCAF bromodomain (yellow) in complex with **(*R*)-23** (yellow) highlighting Trp745. Hydrogen-bonds are shown as red dashed lines and selected water molecules as red spheres.

As observed for fragment **15** in complex with human PCAF (see Figure 4a), the pyridazinone core of **(*R*)-23** sits in the narrow KAc PCAF pocket, forming face-to-face aromatic interactions with Tyr808.[71] As expected, multiple hydrogen-bonds are also observed with interactions to Asn802, Pro746, *via* water to Tyr759 and *via* water to the backbone carbonyl of Glu755. Validating our design hypothesis, the basic piperidine makes a salt bridge to the acidic side chain of Glu755, which presumably contributes to the enhanced potency toward PCAF. Notably there is a subtle movement of Glu755 towards the bound ligand to optimize this favorable salt bridge. (Figure 6b).

Looking to further enhance the PCAF potency, while maintaining the selectivity profile seen with **(*R*)-23**, we targeted substitutions about the piperidine ring. Due to the polarity of **(*R*)-23** (ChromLog$D_{pH7.4}$ 0.6), growing the molecule with more lipophilic groups was considered advantageous for cell permeability. Analysis of the PCAF crystal structure suggested that the 5-

position of the piperidine ring was a suitable vector to access an edge-to-face aromatic interaction with Trp745, which forms part of the PCAF WPF motif (Figure 6c).

Both the *trans*- and the *cis*-diastereomeric 3,5-disubstitued piperidines were accessed *via* alternative routes (Schemes 3 and 4 respectively). The synthesis of the *trans*-diastereomer began with Suzuki-Miyaura cross coupling with commercially available pyridine **24**, followed by trifluoroacetate protection of the pendant aniline to give **25**. Pyridine hydrogenation under forcing conditions was followed by chemoselective Eschweiler-Clarke methylation to give **26**, isolated as a single diastereomer. Amide deprotection, followed by thermal S_NAr reaction with **9** gave target pyridazinone **27** which was determined to be the *trans*-diastereomer by NMR analysis.

Scheme 3[a]

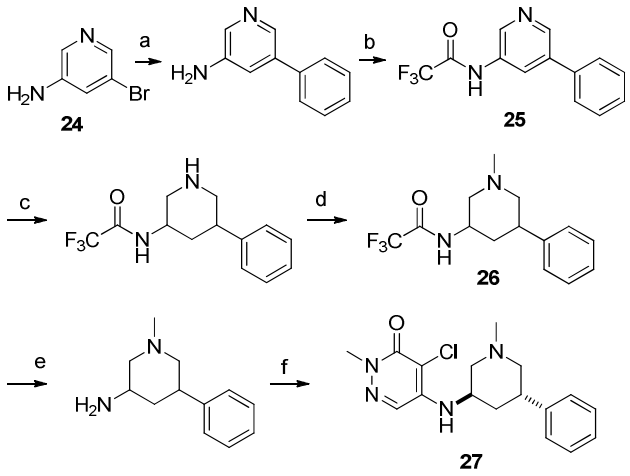

[a]Reagents and conditions: (a) $PhB(OH)_2$, $Pd(PPh_3)_4$, K_2CO_3, PhMe, EtOH, 100 °C, 1 h, 99%; (b) $(CF_3CO)_2O$, CH_2Cl_2, rt, 15 min, 57%; (c) 10% Pd/C. H_2, AcOH, 90 °C, 70 bar, 28%; (d) formaldehyde, HCO_2H, 2-MeTHF, H_2O, 80 °C, 45 min, 86%; (e) K_2CO_3, MeOH, H_2O, rt, 72 h, then 60 °C, 2 h, 99%; (f) 4,5-dichloro-2-methylpyridazinone (**9**), DIPEA, DMSO, 120 °C, 1 h, 27%.

Synthesis of the *cis*-diastereomer began with Curtius rearrangement of readily available nicotinic acid **28** and was followed by a standard Suzuki-Miyaura reaction to give phenyl

substituted pyridine **29** (Scheme 4). Methylation with MeI, was followed by a two stage reduction under forcing conditions to give 3,5-disubtituted piperidine **30** which was isolated as a single diastereomer. Subsequent Boc-deprotection was followed by S_NAr with the appropriate dihalo-substituted pyridazinone. Investigation of **31** by NMR analysis and comparison to the spectra and LCMS retention time of *trans*-diastereomer **27**, revealed only the presence of the *cis*-diastereomer. Subsequent separation of the racemates by preparative chiral HPLC gave the desired single enantiomers **(*R*,*R*)-31**, **(*S*,*S*)-31**, **(*R*,*R*)-32** and **(*S*,*S*)-32**.

Scheme 4[a]

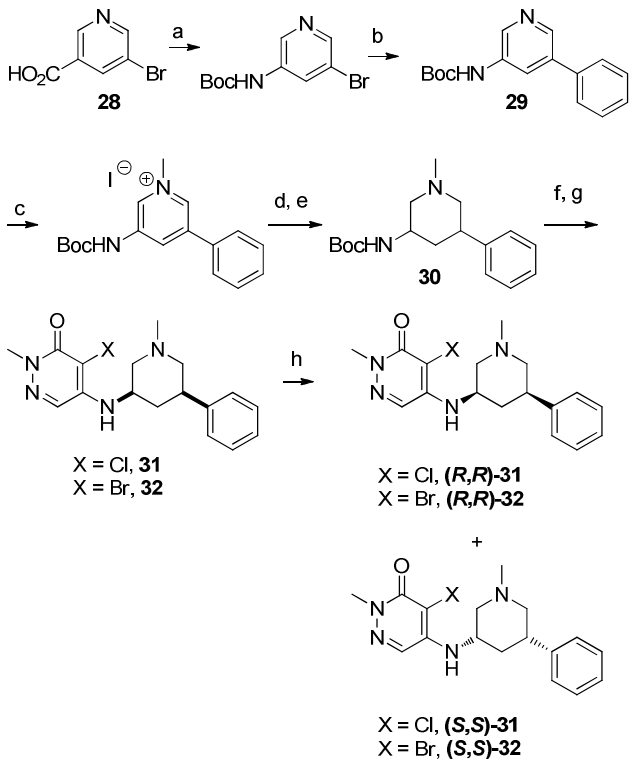

[a]Reagents and conditions: (a) DPPA, *t*-BuOH, NEt_3, PhMe, 100 °C, 2 h, 88%; (b) $PhB(OH)_2$, $Pd(PPh_3)_4$, K_2CO_3, PhMe, EtOH, 100 °C, 1 h, 82%; (c) MeI, DMF, rt, 16 h, 93%; (d) $NaBH_4$, EtOH, 0 °C to rt, 72 h; (e) 10% Pd/C, H_2, MeOH, 60 °C, 50 bar, 24 h, 25% over two steps; (f) TFA, CH_2Cl_2, rt, 16 h; (g) dihalopyridazinone, DIPEA, DMSO, 120-130 °C, 1-10 h; (h) Chiral HPLC purification.

Table 5. 3,5-Disubstituted piperidines[a]

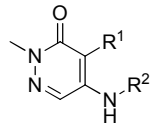

Compound	R^1	R^2	PCAF pIC_{50}	PCAF LE	BRD4 BD1 pIC_{50}	BRD9 pIC_{50}	Δ	Chrom $Log D_{pH7.4}$
(*R*)-23	Cl	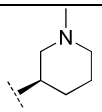	6.3	0.51	<4.3[b]	<4.3	>2.0	0.6
27	Cl	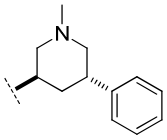	4.4	0.26	<4.3	n.d.	>0.1	4.8
(*R*,*R*)-31	Cl	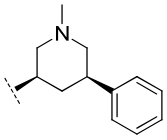	7.1	0.43	<4.3	4.5	>2.8	3.6
(*S*,*S*)-31	Cl	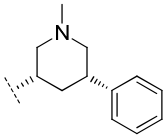	4.6	0.27	<4.3	<4.3	>0.3	3.6
(*R*,*R*)-32	Br	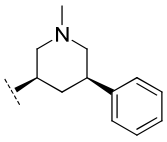	7.4	0.44	<4.3[c]	5.1	>3.1	3.8
(*S*,*S*)-32	Br	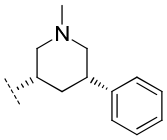	4.9	0.29	<4.3	4.5[d]	>0.6	3.8

[a]LE (1.37 × pIC_{50}) / heavy atom count. Δ = PCAF pIC_{50} – BRD4 BD1 pIC_{50}. n.d.=not determined. For statistics, see Table S1, Supporting information. [b]Data is 7/8 test occasions, pIC_{50} 4.8 1/8 test occasions. [c]Data is 6/8 test occasions, pIC_{50} 4.4 on 2/8 test occasions. [d]Data is 3/4 test occasions, pIC_{50} <4.3 on 1/4 test occasions.

Addition of a phenyl ring to the 5-position of the piperidine ring of **(*R*)-23** to give racemic **27**, with a 3,5-*trans* conformation across the piperidine ring, led to a substantial drop in PCAF potency (Table 5). However, *cis*-diastereomer **(*R*,*R*)-31** had increased PCAF potency compared to **(*R*)-23**, albeit at the expense of some ligand efficiency. As anticipated, selectivity over BRD4

BD1 and BRD9 was observed, with **(*R*,*R*)-31** representing the first compound accessed that achieved the PCAF chemical probe potency criteria set out at the start of our efforts. The majority of the activity was contained in the presumed (*R*,*R*)-enantiomer, with the absolute stereochemistry assigned by analogy to compound **(*R*)-23**.

Properties of Optimized Compounds. Throughout the optimization process, the chloro-pyridazinone had been used, with crystallography of compounds bound to PCAF showing that the halide acted as the methyl mimetic in the KAc binding pocket (see Figures 4 and 6). Intrigued as to whether other halogens would also be tolerated, bromo-analogues **(*R*,*R*)-32** and **(*S*,*S*)-32** were accessed. Comparison of the single point halide change revealed that the bromo-analogues were consistently more potent at PCAF than the chloro-analogues (compare **(*R*,*R*)-31** with **(*R*,*R*)-32** and **(*S*,*S*)-31** with **(*S*,*S*)-32**, Table 4). Pleasingly, **(*R*,*R*)-32** demonstrated 40 nM potency toward PCAF with excellent ligand efficiency and >1000 fold selectivity over BRD4 BD1, albeit with increased activity at BRD9 compared to **(*R*,*R*)-31**. The absolute (*R*,*R*) stereochemistry for **(*R*,*R*)-32** was determined by vibrational circular dichroism and then confirmed by crystallography (*vide infra*). As for chloro-analogue **(*R*,*R*)-31**, the majority of the PCAF potency was retained in a single enantiomer, with the (*S*,*S*)-enantiomer **(*S*,*S*)-32** showing much reduced PCAF activity and potential for use as an enantiomeric negative control.

As highlighted throughout, crystallography of compounds bound to human PCAF had been challenging to achieve. Due to the high bromodomain homology with PCAF (Figure 2c), a GCN5 crystallographic system was also generated. Crystallography of **(*R*,*R*)-32** bound to human GCN5 confirmed not only the binding mode, but also the (*R*,*R*)-absolute stereochemistry across the piperidine ring (Figure 7).

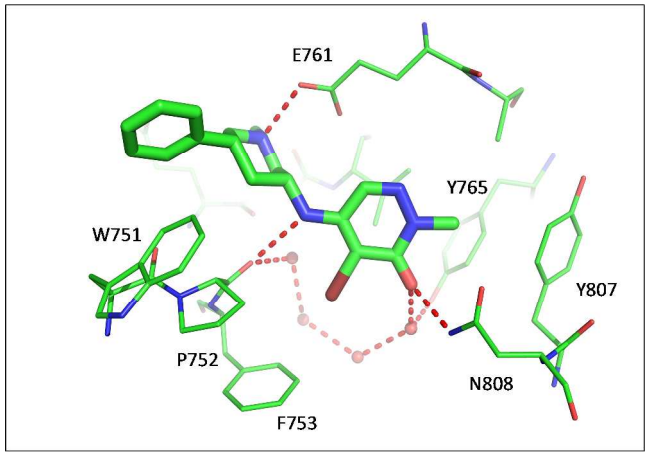

Figure 7. X-ray crystal structure of GCN5 bromodomain (green) in complex with **(*R*,*R*)-32** (green). Hydrogen-bonds are shown as red dashed lines and selected water molecules as red spheres.

As expected based on the previous X-ray crystal structures discussed above, **(*R*,*R*)-32** adopts a similar conformation to piperidine **(*R*)-23** in PCAF, making analogous interactions to Glu761, Asn808, Pro752 and *via* water to Tyr765. When compared to the apo GCN5 structure,[66] Glu761 moves ~2.2Å in order to form a salt bridge with the basic amine. The lipophilic bromo-group is well tolerated as the methyl mimetic and the pendent phenyl ring of **(*R*,*R*)-32** appears to form an edge-to-face interaction with Trp751 which may explain the increased PCAF potency of both **(*R*,*R*)-31** and **(*R*,*R*)-32** observed relative to **(*R*)-23**.

The selectivity of **(*R*,*R*)-32** against the wider bromodomain family was assessed in the BROMO*scan*[72] panel (Figure 8a).

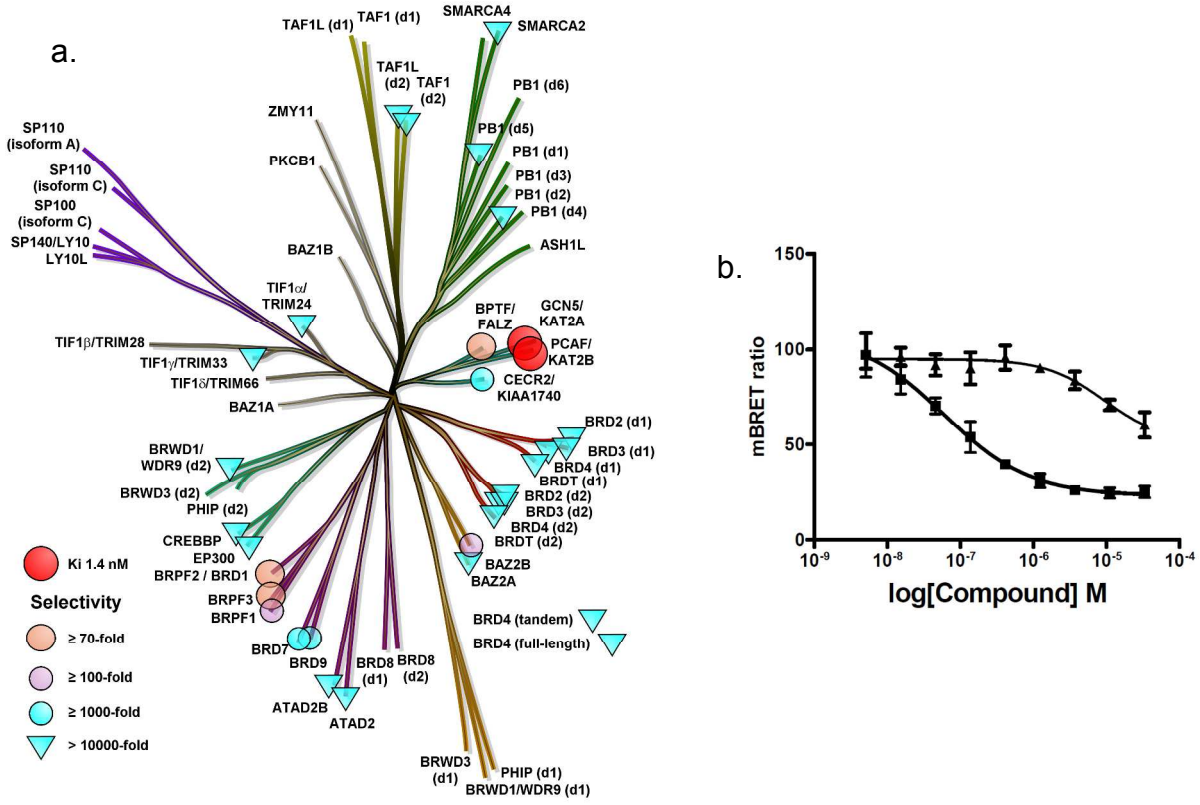

Figure 8. (a) BROMO*scan* data for **(*R*,*R*)-32**, together with fold selectivity relative to PCAF/GCN5 (generated at DiscoveRx Corp.). (b) Full length PCAF cellular NanoBRET dose-response curve of **(*R*,*R*)-32** (squares, pIC_{50} 7.2) and **(*S*,*S*)-32** (triangles, pIC_{50} 5.0). Error bars=SD.

As expected due to high bromodomain homology, compound **(*R*,*R*)-32** showed equipotent activity against PCAF and GCN5 with K_i 1.4 nM for both bromodomains (for full data, see Supporting Information). Confirming the BRD4 BD1 TR-FRET data, exceptional levels of selectivity over the BET family was observed with ≥18000 fold selectivity. ≥70 fold selectivity was observed over every other bromodomain screened, with the closest off target activity at BRPF3 (K_i 100 nM). The difference in observed PCAF potency between the TR-FRET and BROMO*scan* assays may be due to the use of a different detection system, alternate protein constructs and/or the sample preparation methods.

Additional cross screening against an internal GSK panel of 53 biochemical and phenotypic assays considered as potential liabilities did not reveal any off target binding < 3 μM.

Critically for a bromodomain chemical probe, cellular target engagement of PCAF and disruption of chromatin binding was demonstrated through a NanoBRET[73] assay measuring displacement of NanoLuc-tagged full length PCAF from Halo-tagged histone H3.3 (Promega) (Figure 8b). As expected due to the encouraging measured artificial membrane permeability (500 nm/s), treatment of HEK293 cells with **(*R*,*R*)-32** displaced full length PCAF from histone H3.3 with little drop-off from the biochemical assay and a pIC_{50} 7.2 (IC_{50} 60 nM). In comparison and consistent with the biochemical data, enantiomeric negative control **(*S*,*S*)-32** was far less effective at displacing PCAF with a pIC_{50} 5 (IC_{50} 10 μM).

Based on the high PCAF/GCN5 affinity, excellent selectivity against both the wider bromodomain family and a broader selection of targets, high solubility, high permeability and proof of cellular target engagement, **(*R*,*R*)-32** (GSK4027) was chosen as a PCAF/GCN5 bromodomain chemical probe, together with **(*S*,*S*)-32** (GSK4028) as the enantiomeric negative control.[74] A summary of both compounds is given in Table 6.

Table 6. Summary of properties for **(*R*,*R*)-32** and **(*S*,*S*)-32**[a]

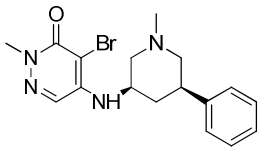

(*R*,*R*)-32 (GSK4027)

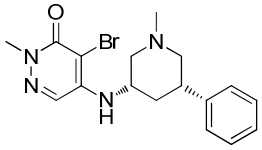

(*S*,*S*)-32 (GSK4028)

	(*R*,*R*)-32	**(*S*,*S*)-32**
PCAF TR-FRET pIC_{50}	7.4	4.9
PCAF BROMO*scan* pK_i	8.9	n.d.
GCN5 BROMO*scan* pK_i	8.9	n.d.
PCAF NanoBRET pIC_{50}	7.2	5.0
BRD4 BD1 TR-FRET pIC_{50}	<4.3[b]	<4.3
BROMO*scan* selectivity	BETs ≥×18000	n.d.

	All others ≥×70	
ChromLog$D_{pH7.4}$/LogP	3.8/4.1	3.8/4.1
CLND solubility (μM)	395	363
AMP (nm/s, pH 7.4)	500	473

[a]For statistics, see Table S1, Supporting information; n.d.= not determined. [b]Data is 6/8 test occasions, pIC_{50} 4.4 on 2/8 test occasions.

CONCLUSION

In conclusion, we report the development of **(*R*,*R*)-32** as a chemical probe for the PCAF/GCN5 bromodomain, together with the enantiomeric negative control **(*S*,*S*)-32**. The probe was optimized from a non-selective, weakly active pyridazinone hit through iterative medicinal chemistry design hypotheses and guided by crystallography where available. Critical to the success of this endeavor was targeting an interaction with Glu756 in PCAF which required specific placement of a basic centre. With high potency against the PCAF/GCN5 bromodomain, exceptional selectivity over the BET bromodomain family and proof of cellular target engagement, we believe **(*R*,*R*)-32** and **(*S*,*S*)-32** represent an important novel addition to the chemical probe toolset and hope these compounds will aid the scientific community in elucidating the biological phenotype of PCAF/GCN5 bromodomain inhibition.

EXPERIMENTAL SECTION

Physicochemical Properties. Artificial membrane permeability, chromatographicLog*D* at pH 7.4, and CLND aqueous solubility were measured using published protocols.[75]

Chemistry. See Supporting Information for general experimental details.

The purity of all compounds tested was determined by LCMS and ^{1}H NMR to be > 95%.

SELECTED EXPERIMENTAL PROCEDURES

***t*ert-Butyl (5-phenylpyridin-3-yl)carbamate (29).** Step 1: Diphenyl phosphorylazide (40.0 mL, 186 mmol) was added dropwise over 15 min to a stirred solution triethylamine (51.5 mL, 371 mmol) and 5-bromonicotinic acid (25 g, 124 mmol) in toluene (250 mL) and *tert*-butanol (50 mL) at rt under N_2. The resultant solution was stirred at rt for 20 min and then heated to 100 °C for 2 h. Upon cooling to rt, sat. aq. $NaHCO_3$ (200 mL) and EtOAc (200 mL) were added. The separated aqueous phase was extracted with EtOAc (2 × 100 mL). The combined organic phase was washed with brine (100 mL), passed through a hydrophobic frit and evaporated under reduced pressure to give an orange solid. The solid was loaded in CH_2Cl_2 and purified by silica gel chromatography using a gradient of 0-15% EtOAc / cyclohexane. The appropriate fractions were combined and evaporated under vacuum to give *tert*-butyl (5-bromopyridin-3-yl)carbamate as a white solid (29.81 g, 88%). ^{1}H NMR (400 MHz, $CDCl_3$) δ 8.34 (s, 1H), 8.30 (app. s, 2H), 6.68 (br.s, 1H), 1.53 (s, 9H); LCMS (formic) $(M+H)^+$ = 273.0, 275.0, R_t = 1.04 min (100%). Step 2: $Pd(PPh_3)_4$ (2.52 g, 2.183 mmol) was added in a single portion to a stirred suspension of *tert*-butyl (5-bromopyridin-3-yl)carbamate (29.81 g, 109 mmol), phenylboronic acid (15.97 g, 131 mmol) and potassium carbonate (45.3 g, 327 mmol) in toluene (250 mL) and EtOH (250 mL) at rt under N_2. The resultant suspension was evacuated under vacuum and then back-filled with N_2 three times. The suspension was then heated to 100 °C for 1 h. Upon cooling to rt, EtOAc (300 mL) and H_2O (200 mL) were added. The separated aqueous phase was extracted with EtOAc (2 × 100 mL), the combined organic phase was passed through a hydrophobic frit and evaporated under reduced pressure to give an orange solid. The solid was mostly dissolved in CH_2Cl_2 (100 mL) and loaded onto a silica plug (15 cm x 30 cm). The plug was eluted with EtOAc (1000 mL). The eluent was combined and evaporated under reduced pressure to give a yellow solid. The solid was suspended in Et_2O (100 mL) and filtered. The collected solid was

washed with Et_2O (200 mL) and air dried under vacuum for 10 min to give **29** as a cream solid (24.29 g, 82%). ^{1}H NMR (400 MHz, $CDCl_3$) δ 8.53 (d, *J* = 2.0 Hz, 1H), 8.40 (d, *J* = 2.4 Hz, 1H), 8.25 (br.s, 1H), 7.62–7.59 (m, 2H), 7.48–7.38 (m, 3H), 6.73 (br.s, 1H), 1.54 (s, 9H); LCMS (formic) $(M+H)^+$ = 271.1, R_t = 0.95 min (100%).

***tert*-Butyl-1-methyl-5-phenylpiperidin-3-yl)carbamate (30).** Step 1: MeI (6.74 ml, 108 mmol) was added dropwise over 2 min to a stirred solution of *tert*-butyl (5-phenylpyridin-3-yl)carbamate (**29**) (24.29 g, 90 mmol) in DMF (125 ml) at rt. The resultant solution was stirred at rt for 16 h by which time a suspension had formed. The suspension was diluted with Et_2O (100 mL) and filtered. The collected solid was washed with Et_2O (2 × 100 mL) and air dried under vacuum for 10 min to give 3-((*tert*-butoxycarbonyl)amino)-1-methyl-5-phenylpyridin-1-ium iodide as a pale yellow solid (34.36 g, 93%). ^{1}H NMR (400 MHz, DMSO-d_6) δ 10.53 (s, 1H), 9.08 (d, *J* = 7.3 Hz, 2H), 8.50 (s, 1H), 7.79–7.76 (m, 2H), 7.66–7.59 (m, 3H), 4.41 (s, 3H), 1.54 (s, 9H); LCMS (formic) $(M)^+$ = 285.1, R_t = 0.78 min (100%). Step 2: Sodium borohydride (0.529 g, 13.97 mmol) was added portionwise over 1 min to a stirred suspension of 3-((*tert*-butoxycarbonyl)amino)-1-methyl-5-phenylpyridin-1-ium iodide (1.44 g, 3.49 mmol) in EtOH (30 mL) at rt. The resultant suspension was stirred at rt for 20 h and then sat. aq. $NaHCO_3$ (50 mL) was added, followed by EtOAc (50 mL). The separated aqueous phase was extracted with EtOAc (2 × 50 mL), the combined organic phase was passed through a hydrophobic frit and evaporated under reduced pressure to give a crude pale yellow oil (890 mg) which was used without further purification. LCMS (formic) $(M+H)^+$ = 287.2, R_t = 0.69 min (33%). Step 3: A solution of the pale yellow oil (890 mg) in MeOH (20 mL) was hydrogenated using the H-cube (settings: 60 °C, 50 bar H_2, 1ml/min flow rate) and 10% Pd/C CatCart 30 as the catalyst. The

solution was recycled through the H-cube for 24 h. The solvent was then evaporated to give a colourless oil. The oil was loaded in CH_2Cl_2 and purified by silica gel column chromatography using a gradient of 0-10% 2 M NH_3 in MeOH / CH_2Cl_2. The appropriate fractions were combined and evaporated under vacuum to give **30** as a colourless oil (405 mg, 45% over two steps). ^{1}H NMR (400 MHz, $CDCl_3$) δ 7.39–7.29 (m, 2H), 7.24–7.20 (m, 3H), 4.38 (br.s, 1H), 3.83 (br.s, 1H), 3.16–3.15 (m, 1H), 2.98–2.92 (m, 1H), 2.33 (s, 3H), 2.26–2.20 (m, 1H), 1.97–1.91 (m, 1H), 1.71–1.45 (m, 11 H), 1.30–1.21 (m, 1H); LCMS (formic) $(M+H)^+$ = 291.2, R_t = 0.71 min (81%).

4,5-Dibromo-2-methylpyridazin-3(2H)-one. Methylhydrazine (1.75 mL, 38.8 mmol) was added dropwise over 5 min to a stirred solution of 3,4-dibromo-5-hydroxyfuran-2(5H)-one (10 g, 38.8 mmol) in EtOH (45 mL) at 0 °C. Following stirring at 0 °C for 1 h, the flask was removed from the cooling bath and heated to 80 °C for 4 h. Upon cooling to rt, the resultant solution was allowed to stand at rt for 12 h by which time a suspension had formed. The suspension was filtered, washed with EtOH (100 mL) and then dried under vacuum for 20 min to give 4,5-dibromo-2-methylpyridazin-3(2H)-one as a pale yellow solid (5.32 g, 51%). ^{1}H NMR (400 MHz, DMSO-d_6) δ 8.12 (s, 1H), 3.67 (s, 3H); LCMS (formic) $(M+H)^+$ = 266.7, 268.7, 270.8, R_t = 0.71 min (100%).

4-Bromo-2-methyl-5-(((3*R,5*R**)-1-methyl-5-phenylpiperidin-3-yl)amino)pyridazin-3(2H)-one (32).** Step 1: TFA (1.85 mL, 24.04 mmol) was added portionwise over 30 s to a stirred solution of *tert*-butyl (1-methyl-5-phenylpiperidin-3-yl)carbamate (698 mg, 2.40 mmol) in CH_2Cl_2 (20 mL) at rt. Following stirring at rt for 1 h the solvent was evaporated under

reduced pressure to give an orange oil. The oil was dissolved in MeOH (20 mL) and then passed through an amino propyl column (10 g) that had been prewashed with MeOH (2 CV). The column was then further eluted with MeOH (2 CV). The appropriate fractions were combined and evaporated under reduced pressure to give crude 1-methyl-5-phenylpiperidin-3-amine as a yellow foam (580 mg) which was used without further purification. Step 2: DIPEA (0.72 mL, 4.11 mmol) was added in a single portion to a stirred solution of 4,5-dibromo-2-methylpyridazin-3(2H)-one (550 mg, 2.05 mmol) and the yellow foam (crude 1-methyl-5-phenylpiperidin-3-amine) (580 mg) in DMSO (10 mL) at rt. The vial was sealed and then heated in a Biotage Initiator microwave to 120 °C for 7 h. Upon cooling to rt, the vial was reheated in a Biotage Initiator microwave to 130 °C for 3 h. Upon cooling to rt, the solution was purified by MDAP (high pH). The solvent was evaporated under vacuum to give **32** as a pale yellow solid (141 mg, 18% over two steps). ^{1}H NMR (400 MHz, DMSO-d_6) δ 7.87 (s, 1H), 7.33–7.20 (m, 5H), 5.81 (d, J = 9 Hz, 1H), 3.96–3.90 (m, 1H), 3.59 (s, 3H), 2.97–2.92 (m, 2H), 2.84 (d, J = 10.8 Hz, 1H), 2.24 (s, 3H), 2.03–1.87 (m, 3 H), 1.73 (q, J = 12 Hz, 1H); LCMS (high pH) $(M+H)^+$ = 377.2, 379.2, R_t = 0.94 min (100%).

4-Bromo-2-methyl-5-(((3*R*,5*R*)-1-methyl-5-phenylpiperidin-3-yl)amino)pyridazin-3(2H)-one [(*R*,*R*)-32] and 4-bromo-2-methyl-5-(((3*S*,5*S*)-1-methyl-5-phenylpiperidin-3-yl)amino)pyridazin-3(2H)-one [(*S*,*S*)-32]. 4-Bromo-2-methyl-5-(((3*R**,5*R**)-1-methyl-5-phenylpiperidin-3-yl)amino)pyridazin-3(2H)-one (**32**) (140 mg) was dissolved in EtOH/heptane (1:1, 2 mL). The solution was purified by preparative chiral HPLC, 30% EtOH/heptanes, 30 mL / min, wavelength 215 nm, 30mm x 25 cm Chiralpak AD-H (Lot No. ADH12143-01). The

appropriate fractions were evaporated under reduced pressure to give **(*R*,*R*)-32** (46 mg) and **(*S*,*S*)-32** (47 mg) as white solids.

(*R*,*R*)-32: m.p. 86–88 °C; ^{1}H NMR (500 MHz, DMSO-d_6) δ 7.87 (s, 1H), 7.33–7.20 (m, 5H), 5.81 (d, J = 9.1 Hz, 1H), 3.97–3.93 (m, 1H), 3.59 (s, 3H), 2.97–2.93 (m, 2H), 2.84 (dd, J = 10.8, 3.2 Hz, 1H), 2.24 (s, 3H), 2.02–1.87 (m, 3 H), 1.73 (q, J = 12.1 Hz, 1H); ^{13}C NMR (125.8 MHz, DMSO-d_6) δ 157.0, 145.5, 143.2, 128.4, 127.0, 126.4, 126.2, 97.3, 61.5, 59.8, 49.4, 45.5, 40.6, 39.6, 36.8; HRMS $(M + H)^+$ calculated for $C_{17}H_{22}BrN_4O$ 377.0972; found 377.0971; LCMS (high pH) $(M+H)^+$ = 377.2, 379.2, R_t = 0.94 min (100%); HPLC (Chiralpak AD-H column, 4.6 mm x 25 cm, 30% EtOH/heptanes, 1 mL/min): 8.1 min (major enantiomer), 13.6 min (minor enantiomer), >99% ee.

(*S*,*S*)-32: Analytical data as **32** above; HPLC (Chiralpak AD-H column, 4.6 mm x 25 cm, 30% EtOH/heptanes, 1 mL/min): 8.1 min (minor enantiomer), 13.6 min (major enantiomer), 97.4% ee.

ASSOCIATED CONTENT

Supporting Information. Additional text describing all biochemical methods and results, all chemistry experimental procedures, full BROMO*scan* and selectivity data for **(*R*,*R*)-32** and X-ray data collection and refinement statistics. This material is available free of charge *via* the Internet http://pubs.acs.org.

Accession Codes: Coordinates have been deposited with the Protein Data Bank under accession codes 5mkx (PCAF/**15** complex), 5ml0 (mouse PCAF/**(*R*)-23** complex), 5mli (BRD4 BD1/**15** complex), 5mkz (BRD4 BD1/**12** complex), 5mky (BRD9/**20** complex) and 5mlj

(GCN5/**(*R*,*R*)-32** complex). Authors will release atomic coordinates and experimental data upon article publication.

AUTHOR INFORMATION

Corresponding Author

*E-mail: philip.g.humphreys@gsk.com. Phone: +44 (0)1438 764252. Fax: +44 (0)1438 766607.

Present Addresses

T.G.H.: Oncology Innovative Medicines and Early Development, AstraZeneca, Cambridge Science Park, Milton Road, Cambridge CB4 0WG, United Kingdom.

J.H.: Dotmatics, The Old Monastery, Windhill, Bishops Stortford, Hertfordshire, CM23 2ND, United Kingdom.

Author Contributions

The manuscript was written through contributions of all authors. All authors have given approval to the final version of the manuscript.

ACKNOWLEDGMENT

Thanks are due to Jacqui Méndez and Danette Daniels of Promega Corporation for facilitating the NanoBRET assay. Heather Barnett for array support, Eric Hortense and Steve Jackson for chiral purification, Douglas Minick for vibrational CD and Steve Richards and Richard Upton for assistance with NMR. Additionally, thanks are due to Emmanuel Demont for helpful discussions throughout the course of this work.

ABBREVIATIONS

AMP, artificial membrane permeability; ATAD2, ATPase family, AAA domain containing 2; BET, bromodomain and extra terminal domain; BRD4 BD1, bromodomain containing protein 4, first bromodomain; BRD9, bromodomain containing protein 9; BRPF3, bromodomain and PHD finger containing 3; CECR2, cat eye syndrome chromosome region, candidate 2; CLND, chemiluminescent nitrogen detection; CREBBP, cAMP response element binding protein binding protein; EP300, E1A-binding protein, 300 kDa; GCN5, general control non-derepressible 5; KAc, acetylated lysine; KAT2, lysine acetyl-transferase 2; LE, ligand efficiency; PCAF, p300/CBP-associated factor; $pIC_{50} = -\log_{10} (IC_{50})$; THIQ, 1,2,3,4-tetrahydroisoquinoline.

REFERENCES

(1) Chung, C.-W. Small molecule bromodomain inhibitors: extending the druggable genome. *Prog. Med. Chem.* **2012**, *51*, 1–55.

(2) Vidler, L. R.; Brown, N.; Knapp, S.; Hoelder, S. Druggability analysis and structural classification of bromodomain acetyl-lysine binding sites. *J. Med. Chem.* **2012**, *55*, 7346–7359.

(3) Nicodeme, E.; Jeffrey, K. L.; Schaefer, U.; Beinke, S.; Dewell, S.; Chung, C.-W.; Chandwani, R.; Marazzi, I.; Wilson, P.; Coste. H.; White, J.; Kirilovsky, J.; Rice, C. M.; Lora, J. M.; Prinjha, R. K.; Lee, K.; Tarakovsky, A. A. Suppression of inflammation by a synthetic histone mimic. *Nature* **2010**, *468*, 1119–1123.

(4) Filippalopoulos, P.; Qi, J.; Picaud, S.; Shen, Y.; Smith, W. B.; Fedorov, O.; Morse, E. M.; Keates, T.; Hickman, T. T.; Felletar, I.; Philpott, M.; Munro, S.; McKeown, M. R.; Wang, Y.; Christie, A. L.; West. N.; Cameron. M. J.; Schwartz, B.; Heightman, T. D.; La Thangue, N.;

French, C. A.; Wiest, O.; Kung, A. L.; Knapp, S.; Bradner, J. E. Selective inhibition of BET bromodomains. *Nature* **2010**, *468*, 1067–1073.

(5) Prinjha, R. K.; Witherington, J.; Lee, K. Place your BETs: the therapeutic potential of bromodomains. *Trends Pharmacol. Sci.* **2012**, *33*, 146−153.

(6) Müller, S.; Filippakopoulos, P.; Knapp, S. Bromodomains as therapeutic targets. *Expert Rev. Mol. Med.* **2011**, *13*, 1−21.

(7) Brand, M.; Measures, A. M.; Wilson, B. G.; Cortopassi, W. A.; Alexander, R.; Höss, M.; Hewings, D. S.; Rooney, T. P. C.; Paton, R. S.; Conway, S. J. Small molecule inhibitors of bromodomain-acetyllysine interactions. *ACS Chem. Biol.* **2015**, *10*, 22−39.

(8) Zhang, G.; Smith, S. G.; Zhou, M.-M. Discovery of chemical inhibitors of human bromodomains. *Chem. Rev.* **2015**, *115*, 11625–11668.

(9) Galdeano, C.; Ciulli, A. Selectivity on-target of bromodomain chemical probes by structure-guided medicinal chemistry and chemical biology. *Future Med. Chem.* **2016**, *8*, 1655–1680.

(10) Romero, F. A.; Taylor, A. M.; Crawford, T. D.; Tsui, V.; Côté, A.; Magnuson, S. Disrupting acetyl-lysine recognition: progress in the development of bromodomain inhibitors. *J. Med. Chem.* **2016**, *59*, 1271–1298.

(11) Müller, S. Targeting the Bromome: are we there yet? *Future Med. Chem.* **2016**, *8*, 1529–1532.

(12) Müller, S.; Brown, P. J. Epigenetic chemical probes. *Clin. Pharmacol. Ther.* **2012**, *92*, 689–693.

(13) Arrowsmith, C. H.; Audia, J. E.; Austin, C.; Baell, J.; Bennett, J.; Blagg, J.; Bountra, C.; Brennan, P. E.; Brown, P. J.; Bunnage, M. E.; Buser-Doepner, C.; Campbell, R. M.; Carter, A. J.; Cohen, P.; Copeland, R. A.; Cravatt, B.; Dahlin, J. L.; Dhanak, D.; Edwards, A. M.; Frederiksen, M.; Frye, S. V.; Gray, N.; Grimshaw, C. E.; Hepworth, D.; Howe, T.; Huber, K. V. M.; Jin, J.; Knapp, S.; Kotz, J. D.; Kruger, R. G.; Lowe, D.; Mader, M. M.; Marsden, B.; Mueller-Fahrnow, A.; Müller, S.; O; Hagan, R. C.; Overington, J. P.; Owen, D. R.; Rosenberg, S. H.; Ross, R.; Roth, B.; Schapira, M.; Schreiber, S. L.; Shoichet, B.; Sundström, M.; Superti-Furga, G.; Taunton, J.; Toledo-Sherman, L.; Walpole, C.; Walters, M. A.; Wilson, T. M.; Workman, P.; Young, R. N.; Zuercher, W. J. The promise and peril of chemical probes. *Nat. Chem. Biol.* **2015**, *11*, 536–541.

(14) Picaud, S.; Fedorov, O.; Thanasopoulou, A.; Leonards, K.; Jones, K.; Meier, J.; Olzscha, H.; Monteiro, O.; Martin, S.; Philpott, M.; Tumber, A.; Filippakopoulos, P.; Yapp, C.; Wells, C.; Che, K. H.; Bannister, A.; Robson, S.; Kumar, U.; Parr, N.; Lee, K.; Lugo, D.; Jeffrey, P.; Taylor, S.; Vecellio, M. L.; Bountra, C.; Brennan, P. E.; O'Mahony, A.; Velichko, S.; Müller, S.; Hay, D.; Daniels, D. L.; Urh, M.; La Thangue, N. B.; Kouzarides, T.; Prinjha, R.; Schwaller J.; Knapp, S. Generation of a selective small molecule inhibitor of the CBP/p300 bromodomain for leukemia therapy *Cancer Res.* **2015**, *75*, 5106–5119.

(15) Hay, D. A.; Fedorov, O.; Martin, S.; Singleton, D. C.; Tallant, C.; Wells, C.; Picaud, S.; Philpott, M.; Monteiro, O. P.; Rogers, C. M.; Conway, S. J.; Rooney, T. P. C.; Tumber A.; Yapp,

C.; Filippakopoulos, P.; Bunnage, M. E.; Müller, S.; Knapp, S.; Schofield, C. J.; Brennan, P. E. Discovery and optimization of small-molecule ligands for the CBP/p300 bromodomains. *J. Am. Chem. Soc.* **2014**, *136*, 9308–9319.

(16) Chekler, E. L. P.; Pellegrino, J. A.; Lanz, T. A.; Denny, R. A.; Flick, A. C.; Coe, J.; Langille, J.; Basak, A.; Liu, S.; Stock, I. A.; Sahasrabudhe, P.; Bonin, P. D.; Lee, K.; Pletcher M. T.; Jones, L. H. Transcriptional profiling of a selective CREB binding protein bromodomain inhibitor highlights therapeutic opportunities *Chem. Biol.* **2015**, *22*, 1588–1596.

(17) Unzue, A.; Xu, M.; Dong, J.; Wiedmer, L.; Spiliotopoulos, D.; Caflisch A.; Nevado, C. Fragment-based design of selective nanomolar ligands of the CREBBP bromodomain *J. Med. Chem.* **2016**, *59*, 1350–1356.

(18) Taylor, A. M.; Côté, A.; Hewitt, M. C.; Pastor, R.; Leblanc, Y.; Nasveschuk, C. G.; Romero, F. A.; Crawford, T. D.; Cantone, N.; Jayaram, H.; Setser, J.; Murray, J.; Beresini, M. H.; de Leon Boenig, G.; Chen, Z.; Conery, A. R.; Cummings, R. T.; Dakin, L. A.; Flynn, E. M.; Huang, O. W.; Kaufman, S.; Keller, P. J.; Kiefer, J. R.; Lai, T.; Li, Y.; Liao, J.; Liu, W.; Lu, H.; Pardo, E.; Tsui, V.; Wang, J.; Wang, Y.; Xu, Z.; Yan, F.; Yu, D.; Zawadzke, L.; Zhu, X.; Zhu, X.; Sims, R. J.; Cochran, A. G.; Bellon, S.; Audia, J. E.; Magnuson, S.; Albrecht, B. K. Fragment-based discovery of a selective and cell active benzodiazepinone CBP/EP300 bromodomain inhibitor (CPI-637). *ACS Med. Chem. Lett.* **2016**, *7*, 531–536.

(19) Crawford, T. D.; Romero, F. A.; Lai, K. W.; Tsui, V.; Taylor, A. M.; Boenig, G. D. L.; Noland, C. L.; Murray, J.; Ly, J.; Choo, E. F.; Hunsaker, T. L.; Chan, E. W.; Merchant, M.; Kharbanda, S.; Gascoigne, K. E.; Kaufman, S.; Beresini, M. H.; Liao, J.; Liu, W.; Chen, K. X.;

Chen, Z.; Conery, A. R.; Côté, A.; Jayaram, H.; Jiang, Y.; Kiefer, J. R.; Kleinheinz, T.; Li, Y.; Maher, J.; Pardo, E.; Poy, F.; Spillane, K. L.; Wang, F.; Wang, J.; Wei, X.; Xu, Z.; Xu, Z.; Yen, I.; Zawadzke, L.; Zhu, X.; Bellon, S.; Cummings, R.; Cochran, A. G.; Albrecht, B. K.; Magnuson, S. Discovery of a potent and selective in vivo probe (GNE-272) for the bromodomains of CBP/EP300. *J. Med. Chem.* **2016**, DOI: 10.1021/acs.jmedchem.6b01022.

(20) Clark, P. G.; Vieira, L. C.; Tallant, C.; Fedorov, O.; Singleton, D. C.; Rogers, C. M.; Monteiro, O. P.; Bennett, J. M.; Baronio, R.; Müller, S.; Daniels, D. L.; Mendez, J.; Knapp, S.; Brennan, P. E.; Dixon, D. J. LP99: discovery and synthesis of the first selective BRD7/9 bromodomain inhibitor. *Angew. Chem., Int. Ed.* **2015**, *54*, 6217−6221.

(21) Martin, L. J.; Koegl, M.; Bader, G.; Cockcroft, X.-L.; Fedorov, O.; Fiegen, D.; Gerstberger, T.; Hofmann, M. H.; Hohmann, A. F.; Kessler, D.; Knapp, S.; Knesl, P.; Kornigg, S.; Müller, S.; Nar, H.; Rogers, C.; Rumpel, K.; Schaaf, O.; Steurer, S.; Tallant, C.; Vakoc, C. R.; Zeeb, M.; Zoephel, A.; Pearson, M.; Boehmelt, G.; McConnell, D. Structure-based design of an in vivo active selective BRD9 inhibitor. *J. Med. Chem.* **2016**, *59*, 4462–4475.

(22) Hay, D. A.; Rogers, C. M.; Fedorov, O.; Tallant, C.; Martin, S.; Monteiro, O. P.; Müller, S.; Knapp, S.; Schofield, C. J.; Brennan, P. E. Design and synthesis of potent and selective inhibitors of BRD7 and BRD9 bromodomains. *Med. Chem. Commun.* **2015**, *6*, 1381–1386.

(23) Theodoulou, N. H.; Bamborough, P.; Bannister, A. J.; Becher, I.; Bit, R. A.; Che, K. H.; Chung, C.-W.; Dittmann, A.; Drewes, G.; Drewry, D. H.; Gordon, L.; Grandi, P.; Leveridge, M.; Lindon, M.; Michon, A.-M.; Molnar, J.; Robson, S. C.; Tomkinson, N. C. O.; Kouzarides, T.;

Prinjha, R. K.; Humphreys, P. G. Discovery of I-BRD9, a selective cell active chemical probe for bromodomain containing protein 9 inhibition. *J. Med. Chem.* **2016**, *59*, 1425–1439.

(24) Bamborough, P.; Barnett, H. A.; Becher, I.; Bird, M. J.; Chung, C.-W.; Demont, E. H.; Diallo, H.; Fallon, D.; Gordon, L. J.; Grandi, P.; Hobbs, C. I.; Hooper-Greenhill, E.; Jones, E. J.; Law, R. P.; Le Gall, A.; Lugo, D.; Michon, A.-M.; Mitchell, D. J.; Prinjha, R. K.; Sheppard, R. J.; Watson, A. J. B.; Watson, R. J. GSK6853, a chemical probe for inhibition of the BRPF1 bromodomain. *ACS Med. Chem. Lett.* **2016**, *7*, 552−557.

(25) Bamborough, P.; Chung, C.-W.; Demont, E. H.; Furze, R. C.; Bannister, A. J.; Che, K. H.; Diallo, H.; Douault, C.; Grandi, P.; Kouzarides, T.; Michon, A.-M.; Mitchell, D. J.; Prinjha, R. K.; Rau, C.; Robson, S.; Sheppard, R. J.; Upton, R.; Watson, R. J. A chemical probe for the ATAD2 bromodomain. *Angew. Chem. Int. Ed.* **2016**, *55*, 11382−11386.

(26) Gerstenberger, B. S.; Trzupek, J. D.; Tallant, C.; Fedorov, O.; Filippakopoulos, P.; Brennan, P. E.; Fedele, V.; Martin, S.; Picaud, S.; Rogers, C.; Parikh, M.; Taylor, A.; Samas, B.; O'Mahony, A.; Berg, E.; Pallares, G.; Torrey, A. D.; Treiber, D. K.; Samardjiev, I. J.; Nasipak, B. T.; Padilla-Benavides, T.; Wu, Q.; Imbalzano, A. N.; Nickerson, J. A.; Bunnage, M. E.; Müller, S.; Knapp, S.; Owen, D. R. Identification of a chemical probe for family VIII bromodomains through optimization of a fragment hit. *J. Med. Chem.* **2016**, *59*, 4800−4811.

(27) Theodoulou, N. H.; Tomkinson, N. C. O.; Prinjha, R. K.; Humphreys, P. G. Progress in the development of non-BET bromodomain chemical probes. *ChemMedChem* **2016**, *11*, 477–487.

(28) Moustakim, M.; Clark, P. G. K.; Hay, D. A.; Dixon, D. J.; Brennan, P. E. Chemical probes and inhibitors of bromodomains outside the BET family. *MedChemComm* **2016**, DOI: 10.1039/C6D00373G.

(29) Clark, P. G. K.; Dixon, D. J.; Brennan, P. E. Development of chemical probes for the bromodomains of BRD7 and BRD9. *Drug Discovery Today: Technol.* **2016**, *19*, 73–80.

(30) Palmer, W. S. Development of small molecule inhibitors of BRPF1 and TRIM24 bromodomains. *Drug Discovery Today: Technol.* **2016**, *19*, 65–71.

(31) http://www.thesgc.org/chemical-probes (October 12, 2016)

(32) Sdelci, S.; Lardeau, C.-H.; Tallant, C.; Klepsch, F.; Klaiber, B.; Bennett, J.; Rathert, P.; Schuster, M.; Penz, T.; Fedorov, O.; Superti-Furga, G.; Bock, C.; Zuber, J.; Huber, K. V. M.; Knapp, S.; Müller, S.; Kubicek, S. Mapping the chemical chromatin reactivation landscape identifies BRD4-TAF1 cross-talk. *Nat. Chem. Biol.* **2016**, *12*, 504-510.

(33) Theodoulou, N. H.; Tomkinson, N. C. O.; Prinjha, R. K.; Humphreys, P. G. Clinical progress and pharmacology of small molecule bromodomain inhibitors. *Curr. Opin. Chem. Biol.* **2016**, *33*, 58–66.

(34) Hohmann, A. F.; Martin, L. J.; Minder, J. L.; Roe, J.-S.; Shi, J.; Steurer, S.; Bader, G.; McConnell, D.; Pearson, M.; Gertberger, T.; Gottschamel, T.; Thompson, D.; Suzuki, Y.; Koegl, M.; Vakoc, C. R. Sensitivity and engineered resistance of myeloid leukemia cells to BRD9 inhibition. *Nat. Chem. Biol.* **2016**, *12*, 672–679.

(35) Yang, X.-J.; Ogryzko, V. V.; Nishikawa, J.-I.; Howard, B. H.; Nakatani, Y. A p300/CBP-associated factor that competes with the adenoviral oncoprotein E1A. *Nature* **1996**, *382*, 319–324.

(36) Linares, L. K.; Kiernan, R.; Triboulet, R.; Chable-Bessia, C.; Latreille, D.; Cuvier, O.; Lacroix, M.; Le Cam, L.; Coux, O.; Benkirane, M. Intrinsic ubiquitination activity of PCAF controls the stability of the oncoprotein Hdm2. *Nat. Cell Biol.* **2007**, *9*, 331–338.

(37) Kruidenier, L.; Lee, K.; Tough, D. F.; Wilson, D. M. Inhibitors of bromodomain-containing protein PCAF for the treatment of autoimmune and inflammatory diseases or for the treatment of cancer. WO2014/037362A1, 2014.

(38) Masumi, A.; Wang, I.-M.; Lefebvre, B.; Yang, X.-J.; Nakatani, Y.; Ozato, K. The histone acetylase PCAF is a phorbol-ester-inducible coactivator of the IRF family that confers enhanced interferon responsiveness. *Mol. Cell Biol.* **1999**, *19*, 1810–1820.

(39) Modak, R.; Basha, J.; Bharathy, N.; Maity, K.; Mizar, P.; Bhat, A. V.; Vasudevan, M.; Rao, V. K.; Kok, W. K.; Natesh, N.; Taneja, Kundu, T. K. Probing p300/CBP associated factor (PCAF)-dependent pathways with a small molecule inhibitor. *ACS Chem. Biol.* **2013**, *8*, 1311–1323.

(40) Stimson, L.; Rowlands, M. G.; Newbatt, Y. M.; Smith, N. F.; Raynaud, F. I.; Rogers, P.; Bavetsias, V.; Gorsuch, S.; Jarman, M.; Bannister, A.; Kouzarides, T.; McDonald, E.; Workman, P.; Aherne, G. W. Isothiazolones as inhibitors of PCAF and p300 histone acetyltransferase activity. *Mol. Cancer Ther.* **2005**, *4*, 1521–1532.

(41) Malatesta, M.; Steinhauer, C.; Mohammad, F.; Pandey, D. P.; Squatrito, M.; Helin, K. Histone acetyltransferase PCAF is required for hedgehog-Gli-dependent transcription and cancer cell proliferation. *Cancer Res.* **2013**, *73*, 6323−6333.

(42) Duclot, F.; Meffre, J.; Jacquet, C.; Gongora, C.; Maurice, T. Mice knock out for the histone acetyltransferase p300/CBP binding protein-associated factor develop a resistance to amyloid toxicity. *Neuroscience* **2010**, *167*, 850–863.

(43) Mujtaba, S.; He, Y.; Zeng, L.; Farooq, A.; Carlson, J. E.; Ott, M.; Verdin, E.; Zhou, M. M. Structural basis of lysine-acetylated HIV-1 Tat recognition by PCAF bromodomain. *Mol. Cell* **2002**, 9, 575– 586.

(44) Dorr, A.; Kiermer, V.; Pedal, A.; Rackwitz, H. R.; Henklein, P.; Schubert, U.; Zhou, M. M.; Verdin, E.; Ott, M. Transcriptional synergy between Tat and PCAF is dependent on the binding of acetylated Tat to the PCAF bromodomain. *EMBO J.* **2002**, *21*, 2715–2723.

(45) Jin, Q.; Yu, L.R.; Wang, L.; Zhang, Z.; Kasper, L.H.; Lee, J.E.; Wang, C.; Brindle, P.K.; Dent, S.Y.; Ge, K. Distinct roles of GCN5/PCAF-mediated H3K9ac and CBP/p300-mediated H3K18/27ac in nuclear receptor transactivation. *EMBO J.* **2011**, *30*, 249–262.

(46) Li, S.; Shogren-Knaak, M.A. The GCN5 bromodomain of the SAGA complex facilitates cooperative and cross-tail acetylation of nucleosomes. *J. Biol. Chem.* **2009**, *284*, 9411–9417.

(47) Chen, L.; Wei, T.; Si, X.; Wang, Q.; Li, Y.; Leng, Y.; Deng, A.; Chen, J.; Wang, G.; Zhu, S.; Kang, J. Lysine acetyltransferase GCN5 potentiates the growth of non-small cell lung cancer

via promotion of E2F1, cyclin D1, and cyclin E1 expression. *J. Biol. Chem.* **2013**, *288*, 14510−14521.

(48) Robert, T.; Vanoli, F.; Chiolo, I.; Shubassi, G.; Bernstein, K. A.; Rothstein, R.; Botrugno, O. A.; Parazzoli, D.; Oldani, A.; Minucci, S.; Foiani, M. HDACs link the DNA damage response, processing of double-strand breaks and autophagy. *Nature* **2011**, *471*, 74−79.

(49) Burgess, R. J.; Zhou, H.; Han, J. H.; Zhang, Z. G. A role for Gcn5 in replication coupled nucleosome assembly. *Mol. Cell.* **2010**, *37*, 469−480.

(50) Brownell, J. E.; Zhou, J.; Ranalli, T.; Kobayashi, R.; Edmondson, D. G.; Roth, S. Y.; Allis, C. D. Tetrahymena histone acetyltransferase A: A homolog to yeast Gcn5p linking histone acetylation to gene activation. *Cell* **1996**, *84*, 843−851.

(51) Germaniuk-Kurowska, A.; Nag, A.; Zhao, X.; Dimri, M.; Band, H.; Band, V. Ada3 requirement for HAT recruitment to estrogen receptors and estrogen-dependent breast cancer cell proliferation. *Cancer Res.* **2007**, *67*, 11789–11797.

(52) Chen, J.; Luo, Q.; Yuan, Y.; Huang, X.; Cai, W.; Li, C.; Wei, T.; Zhang, L.; Yang, M.; Liu, Q.; Ye, G.; Dai, X.; Li, B. Pygo2 associates with MLL2 histone methyltransferase and GCN5 histone acetyltransferase complexes to augment Wnt target gene expression and breast cancer stem-like cell expansion. *Mol. Cell. Biol.* **2010**, *30*, 5621–5635.

(53) Nagy, Z.; Tora, L. Distinct GCN5/PCAF-containing complexes function as co-activators and are involved in transcription factor and global histone acetylation. *Oncogene* **2007**, *26*, 5341–5357.

(54) Greenberg, M.L.; Myers, P.L.; Skvirsky, R. C.; Greer, H. New positive and negative regulators for general control of amino acid biosynthesis in Saccharomyces cerevisiae. *Mol. Cell. Biol.* **1986**, *6*,1820–1829.

(55) Skvirsky, R. C.; Greenberg, M. L.; Myers, P. L.; Greer, H. A new negative control gene for amino acid biosynthesis in Saccharomyces cerevisiae. *Curr. Genet.* **1986**, *10*, 495–501.

(56) Syntichaki, P.; Topalidou, I.; Thireos, G. The Gcn5 bromodomain co-ordinates nucleosome remodeling. *Nature* **2000**, *404*, 414–417.

(57) Zeng, L.; Li, J.; Muller, M.; Yan, S.; Mujtaba, S.; Pan, C.; Wang, Z.; Zhou, M.-M. Selective small molecules blocking HIT-1 Tat and coactivator PCAF association. *J. Am. Chem. Soc.* **2005**, *127*, 2376–2377.

(58) Hu, P.; Wang, X.; Zhang, B.; Zhang, S.; Wang, Q.; Wang, Z. Fluorescence polarization for the evaluation of small molecule inhibitors of PCAF BRD/Tat-AcK50 association. *ChemMedChem* **2014**, *9*, 928–931.

(59) Navratilova, I.; Aristotelous, T.; Picaud, S.; Chaikuad, A.; Knapp, S.; Filappakopoulos, P.; Hopkins, A. L. Discovery of new bromodomain scaffolds by biosensor fragment screening. *ACS Med. Chem. Lett.* **2016**, DOI: 10.1021/acsmedchemlett.6b00154.

(60) Chaikaud, A.; Lang, S.; Brennan, P. E.; Temperini, C.; Fedorov, O.; Hollander, J.; Nachane, R.; Abell, C.; Müller, S.; Siegal, G.; Knapp, S. Structure-based identification of inhibitory fragment targeting the p300/CBP-associated factor bromodomain. *J. Med. Chem.* **2016**, *59*, 1648–1653.

(61) Albrecht, B. K.; Cote, A.; Crawford, T.; Duplessis, M.; Good, A. C.; Leblanc, Y.; Magnuson, S.; Nasveschuk, C. G.; Pastor, R.; Romero, F. A.; Taylor, A. M. Phthalazine derivatives of forumula (I) as PCAF and GCN5 inhibitors for use in the treatment of cancer. WO2016/036954A1, 2016.

(62) Albrecht, B. K.; Cote, A.; Crawford, T.; Duplessis, M.; Good, A. C.; Leblanc, Y.; Magnuson, S.; Nasveschuk, C. G.; Pastor, R.; Romero, F. A.; Taylor, A. M. Therapeutic compounds and uses thereof. WO2016/036873A1, 2016.

(63) Albrecht, B. K.; Burdick, D. J.; Cote, A.; Duplessis, M.; Nasveschuk, C. G.; Taylor, A. M. Pyridazinone derivatives and their use in the treatment of cancer WO2016/112298A1, 2016.

(64) Bunnage, M. E.; Piatnitski Chekler, E. L.; Jones, L. H. Target validation using chemical probes. *Nat. Chem. Biol.* **2013**, *9*, 195–199.

(65) Dhalluin, C.; Carlson, J. E.; Zeng, L.; He, C.; Aggarwal, A. K.; Zhou, M.-M. Structure and ligand of a histone acetyltransferase bromodomain. *Nature* **1999**, *399*, 491–496.

(66) Filippakopoulos, P.; Picaud, S.; Mangos, M.; Keates, T.; Lambert, J. P.; Barsyte-Lovejoy, D.; Felletar, I.; Volkmer, R.; Müller, S.; Pawson, T.; Gingras, A. C.; Arrowsmith, C. H.; Knapp, S. Histone recognition and large-scale structural analysis of the human bromodomain family. *Cell* **2012**, *149*, 214–231.

(67) Demont, E. H.; Chung, C.-W.; Furze, R. C.; Grandi, P.; Michon, A.-M.; Wellaway, C.; Barrett, N.; Bridges, A. M.; Craggs, P. D.; Diallo, H.; Dixon, D. P.; Douault, C.; Emmons, A. J.; Jones, E. J.; Karamshi, B. V.; Locke, K.; Mitchell, D. J.; Mouzon, B. H.; Prinjha, R. K.; Roberts,

A. D.; Sheppard, R. J.; Watson, R. J.; Bamborough, P. Fragment-based discovery of low-micromolar ATAD2 bromodomain inhibitors. *J. Med. Chem.* **2015**, *58*, 5649–5673.

(68) The chloro-group of a 3-chloropyridinone has been disclosed as the methyl mimetic when bound to BRD4 BD1, see: Vidler, L. R.; Filippakopoulos, P.; Fedorov, O.; Picaud, S.; Martin, S.; Tomsett, M.; Woodward, H.; Brown, N.; Kanpp, S.; Hoelder, S. Discovery of novel small-molecule inhibitors of BRD4 using structure-based virtual screening. *J. Med. Chem.* **2013**, *56*, 8073–8088.

(69) Polonka-Bálint, A.; Saraceno, C.; Ludányi, K.; Bényei, A.; Mátyus, P. Novel extensions of the *tert*-amino effect: Formation of phenanthridines and diarene-fused azocines from ortho-ortho'-functionalized biaryls. *Synlett* **2008**, 2846–2850.

(70) Dunkel, P.; Túrós, G.; Bényei, A.; Ludányi, K.; Mátyus, P. Synthesis of novel fused azecine ring systems through application of the *tert*-amino effect. *Tetrahedron* **2010**, *66*, 2331–2339.

(71) Due to amino acid differences between the orthologues, mouse PCAF amino acid numbering = human PCAF amino acid numbering – 1.

(72) BROMO*scan* recombinant protein binding assays were carried out at DiscoveRx, http://www.discoverx.com.

(73) Machleidt, T.; Woodroofe, C. C.; Schwinn, M. K.; Méndez, J.; Robers, M. B.; Zimmerman, K.; Otoo, P.; Daniels, D. L.; Kirkland, T. A.; Wood, K. V. NanoBRET-a novel

BRET platform for the analysis of protein-protein interactions. *ACS. Chem. Biol.* **2015**, *10*, 1797–1804.

(74) Upon storage of **(*R*,*R*)-32** as a solid at ambient temperature under laboratory lighting or as a 10 mM DMSO solution at –20 °C under laboratory lighting for >3 years, <5% degradation was observed by LCMS analysis.

(75) Gosmini, R.; Nguyen, V. L.; Toum, J.; Simon, C.; Brusq, J. M.; Krysa, G.; Mirguet, O.; Riou-Eymard, A. M.; Boursier, E. V.; Trottet, L.; Bamborough, P.; Clark, H.; Chung, C.-W.; Cutler, L.; Demont, E. H.; Kaur, R.; Lewis, A. J.; Schilling, M. B.; Soden, P. E.; Taylor, S.; Walker, A. L.; Walker, M. D.; Prinjha, R. K.; Nicodeme, E. The discovery of I-BET726 (GSK1324726A), a potent tetrahydroquinoline ApoA1 up-regulator and selective BET bromodomain inhibitor. *J. Med. Chem.* **2014,** *57,* 8111–8131.

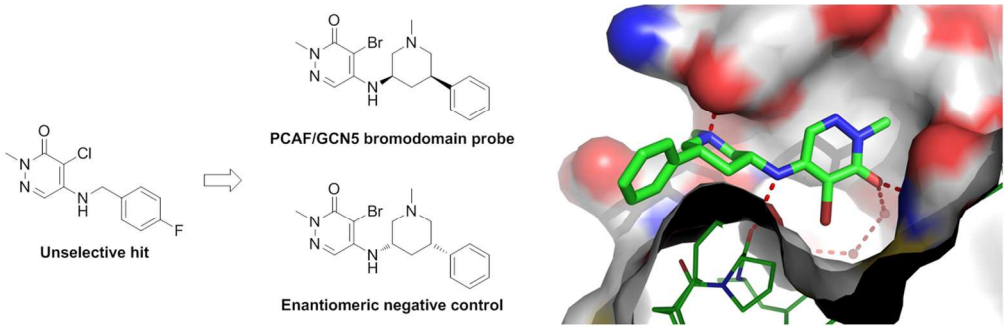

Table of Contents graphic
Table of Contents graphic
355x114mm (96 x 96 DPI)